DEPARTMENT OF THE AIR FORCE

HEADQUARTES, 603D REGIONAL SUPPORT GROUP (USAFE)

European Office of Aerospace Research and Development

(EOARD)

Final Report

Referring to

Grant # 043021, Award # FA8655-04-1-3021

Period of Performance 1 February 2004 to 31 January 2005

Title: **Advanced singlet oxygen generator for a COIL**

Investigators: ***Russian side*:**
M. Zagidullin, V. Nikolaev, M. Svistun, N. Khvatov,
Lebedev Physical Institute RAS, Samara Branch
***Czech side*:**
J. Hrubý, O. Špalek, V. Jirásek, J. Kodymová, M. Čenský
Institute of Physics AS CR

Prime consultant and supervisor:
Dr. Gordon D. Hager
USAF Research Laboratory /DE, Kirtland AFB, NM

Contractor: **Jarmila Kodymová**
Department of Chemical Lasers
Institute of Physics of Academy of Sciences CR
Na Slovance 2
182 21 Prague 8
Czech Republic
Phone: +420 266 052 699
Fax: +420 286 890 265
E-mail: kodym@fzu.cz

Date of submission: **31 January 2005**
12 month after grant award according to Order for Supplies or Services

REPORT DOCUMENTATION PAGE

Form Approved OMB No. 0704-0188

1. REPORT DATE *(DD-MM-YYYY)*	2. REPORT TYPE	3. DATES COVERED *(From – To)*
14-02-2005	Final Report	1 February 2004 - 01-Feb-05

4. TITLE AND SUBTITLE

Advanced Singlet Oxygen Generator for a COIL

5a. CONTRACT NUMBER
FA8655-04-1-3021

5b. GRANT NUMBER

5c. PROGRAM ELEMENT NUMBER

6. AUTHOR(S)

Dr. Jarmila Kodymova

5d. PROJECT NUMBER

5d. TASK NUMBER

5e. WORK UNIT NUMBER

7. PERFORMING ORGANIZATION NAME(S) AND ADDRESS(ES)
Academy of Sciences
Na Slovance 2
Prague 8 182 21
Czech Republic

8. PERFORMING ORGANIZATION REPORT NUMBER

N/A

9. SPONSORING/MONITORING AGENCY NAME(S) AND ADDRESS(ES)

EOARD
PSC 802 BOX 14
FPO 09499-0014

10. SPONSOR/MONITOR'S ACRONYM(S)

11. SPONSOR/MONITOR'S REPORT NUMBER(S)
SPC 04-3021

12. DISTRIBUTION/AVAILABILITY STATEMENT

Approved for public release; distribution is unlimited.

13. SUPPLEMENTARY NOTES

14. ABSTRACT

This report results from a contract tasking Academy of Sciences as follows: The Grantee will develop new and radically different ideas for a high performance, advanced singlet oxygen generator for driving a supersonic COIL. Various ideas for high performance generator concepts matching up to the above prosperities should be theoretically considered and the best concept should be developed into the experimental device of advanced SOG. Phase 1: A conceptualisation of the problem including a literature study, theoretical estimation of particular problems, calculations, elaboration of generator concept. At the end of the first year, a consortium of the supervisor, contractor, and Russian and Czech investigators should evaluate the first phase of project solution, and if it is successful, to specify the advanced generator concept that should be further developed.
Phase 2: A design of advanced generator device including detailed technical drawings, purchasing of suitable constructional materials and experimental equipments, construction and testing of individual parts of experimental set-up, construction of small-scale advanced generator.
Phase 3: A testing of performance parameters of the small-scale advanced generator and characterization of its output parameters (O2(1D) yield, residual chlorine and H2O vapor content), and testing this generator with coupling to the laser.

15. SUBJECT TERMS
EOARD, Chemical oxygen iodine lasers

16. SECURITY CLASSIFICATION OF:			17. LIMITATION OF ABSTRACT	18, NUMBER OF PAGES	19a. NAME OF RESPONSIBLE PERSON
a. REPORT	b. ABSTRACT	c. THIS PAGE			DONALD J SMITH
UNCLAS	UNCLAS	UNCLAS	UL	56	19b. TELEPHONE NUMBER *(Include area code)* +44 (0)20 7514 4953

DECLARATION

(1) The Contractor, Institute of Physics of Academy of Sciences of the Czech Republic, hereby declares that, to the best of its knowledge and believes, the technical data delivered herewith under Contract No. FA8655-04-1-3021 is complete, accurate, and complies with all requirements of the contract.

(2) I certify that there were no subject inventions to declare as defined in FAR 52.227-13, during the performance of this Contract.

Date: 31 January 2005

Name and Title of Principal Investigator: Dr. Jarmila Kodymová

Name and Title of Authorized Official: Dipl. Ing. Karel Jungwirth, DrSc.
Director of Institute of Physics AS CR

CONTENT

Objects and goals of developing an advanced SOG

This one-year EOARD grant was awarded to promote the co-operation of COIL Laboratories at Institutes of Physics in Prague, Czech Republic and Samara, Russia on development new concepts of advanced chemical generator of singlet oxygen for a COIL. The generator should have the following characteristics:

1. A high-pressure operation with ~100 Torr of O_2 partial pressure
2. A single BHP pass burn down (probably requiring a dilute BHP to maintain the thermal control and so to limit H_2O vapor)
3. A close coupling of the generator to the nozzle plenum to minimize $O_2(^1\Delta)$ losses
4. An efficient disengagement of gas/liquid (conceptually involving the angular acceleration of fluid and gas or both)
5. A scalability to be suitable for the airborne and mobile applications

The investigation within the framework of this grant has been aimed at conceptualisation of the problem including a literature study, theoretical estimation of particular problems, calculations, and designing the concept of the experimental device.

A. The conceptual designing of the small-scale Rotating Sparger SOG (RSSOG) (30 mmole/s) with next requirements

1. Estimations of hydrodynamic and mass-transfer rates chlorine utilization and $O_2(^1\Delta)$ yield

1.1. Basic data and formulas

The estimation of RSSOG parameters is based on the simplified liquid-gas hydrodynamic and simplified model of the transport phenomena of the bubbler centrifugal apparatus performed in the interim Report 001 of this grant.

The parameters of RSSOG that should be found for achieving the required parameters of the advanced SOG are presented in **Table 1**.

Tab. 1

1	R	Radius of RSSOG
2	d_0	Diameter of holes
3	H	Height of liquid layer
4	w	Axial BHP velocity
5	n	Revolutions per minute (RPM)
6	U_g	Gas velocity from the nozzle
7	N_H	BHP molarity (KOH)

Tab. 2
Physical-chemical data of the gas and BHP

1	ρ_l	BHP density	1.3 g/cm^3
2	μ_l	BHP viscosity	0.1 g/cm/s
3	K	Rate constant of reaction $Cl_2 + HO_2^- \rightarrow O_2(^1\Delta) + 2Cl^- + H^+$	~5×10^8 M^{-1}s^{-1}
4	H_c	Henry constant	~1
5	D_c	Chlorine diffusion coefficient in BHP	5×10^{-6} cm^2/s
6	D_o	Oxygen diffusion coefficient in BHP	5×10^{-6} cm^2/s
7	D_H	HO_2^- diffusion coefficient in BHP	5×10^{-6} cm^2/s
8	μ_g	Chlorine viscosity	1.6×10^{-4} g/cm/s)
9	D_{cHe}	Chlorine diffusion coefficient in He	300/P(torr) (cm^2/s)
10	D_{cO2}	Chlorine diffusion coefficient in O_2	100/P(torr) (cm^2/s)
11	τ_Δ	Lifetime of $O_2(^1\Delta)$ in the BHP	2×10^{-6}s

Tab. 3

Given and calculated intermediate parameters

1	T=253°K	Input BHP temperature
2	P_0=100 torr	Total pressure (O_2 + Cl_{2resid}) over BHP layer
3	A=0	Dilution with Helium
4	$w_r=\omega R$	Peripheral BHP velocity
5	$G=\omega^2 R$	Centrifugal acceleration
6	$P= P_0 +\omega^2 RH\rho l$	Gas pressure at the nozzle outlet (torr)
7	ρ_g=(P/RT)(71/(1+A)+A*4/(1+A))	Gas density at the nozzle outlet (g/cm^3)
8	N_c=P/RT/(1+A)	Chlorine concentration at the nozzle outlet (mole/cm^3)
9	$\mu_g= 3\times10^{-4}\times A/(1+A)+ 1.6\times10^{-4}/(1+A))$	Gas viscosity (g/cm/s)
10	$D_c^g=((1+A)/P)(A/ 300+ 1/100)^{-1}$	Chlorine diffusion coefficient in O_2-He mixture (cm^2/s)
11	$\mathrm{Re}=\frac{\boldsymbol{\rho_\ell U_0 d_0}}{\boldsymbol{\mu_\ell}}$	Reynolds number for the gas in nozzle

Tab. 4

Estimation of the hydrodynamic parameters of the rotary bubbler, specific chlorine absorption time and $O_2(^1\Delta)$ yield parameters

1	$r = r_0 \times 0.68 \frac{(\rho_\ell/\rho_g)^{0.14}}{1+(\mu_g/\mu_\ell)^{0.32}} \left(\frac{U_g^2}{d_o G}\right)^{0.16}$	Radius of bubble
2	$U \approx 1.43\sqrt{rG}$	Velocity of bubble
3	$\tau = \frac{1}{C}\sqrt{0.12\times10^{-6}C^2 + 1.05\times10^{-3}C + 0.21} - 0.35\times10^{-3}$ $C = \sqrt{\frac{G}{d_0}}\left(\frac{\rho_g d_0 G}{\rho_\ell U_g^2}\right)^{0.1} \mathrm{Re}^{0.06}$	Time of bubble formation
4	$f = \sqrt{0.25\times C^2 + 0.71\times C + 0.19\times10^6} - 0.44\times10^3$	Frequency of bubbles generation
5	$t_r = \tau + H/U$	Bubble residence time in BHP
6	$t_g \approx 0.06 r^2 / D_c^g$	Chlorine absorption time due to gas resistance
7	$t_s \approx H_c r / \left(\sqrt{KN_H D_c}\right)$	Chlorine absorption time according to surface reaction
8	$t_c = 2r/U$	The time of the BHP surface renewal
9	$t_{dep} \approx \left(\frac{N_H}{N_c}\right)^2 \frac{H_c^2}{D_C K N_H} \frac{\pi D_H}{4}$	Time of strong HO_2^- depletion (formation of sheet flame)
10	$t_{ab} = \frac{N_c}{N_H}\left(\frac{r^3}{UD_H}\right)^{0.5}\left(\frac{2\pi}{3}\right)^{0.5}$	Time of total chlorine absorption in sheet flame approximation
11	$Ut = \frac{h}{t_{ab}U}\left[\sqrt{\frac{P}{P_0}} - 1\right]\left(\frac{P}{P-P_0}\right)$	Estimated chlorine utilization for moving bubble (see below)

12	$Y_{det} \approx 0.9\exp\left(-\frac{2N_c}{H_c N_H}\sqrt{\frac{\pi D_c r}{UD_o\tau_\Delta}}\right)$	Estimation of minimal detachment $O_2(^1\Delta)$ yield
13	$P_c t_r = (P+P_0)/(A+1)*t_r/4$	Average $P\tau$ parameter due to homogeneous quenching of $O_2(^1\Delta)$
14	$Y=Y_{det}/(1+Y_{det} P_c t_r)$	Estimation of $O_2(^1\Delta)$ yield
15	$N_n=(2r)^{-2}$	Maximum density of chlorine nozzles ($1/cm^2$) to avoid bubble coalescence
16	$M_c = fN_c \times \frac{4\pi r^3}{3} N_n$	Estimated oxygen flux from the bubble layer ($mmole/cm^2/s$)

Note to Item 11: Estimation of chlorine utilization:

Because of very high initial chlorine pressure (more than 100 torr under BHP layer) and very fast depletion of the HO_2^- ions, the chlorine absorption rate will occur according to the flame sheet approximation. In this approximation the chlorine flow rate to bubble surface will be

$$J_c = \pi\frac{4}{3}N_H D_H\left(\frac{3Ur^3}{2\pi D_H}\right)^{0.5}$$

The chlorine absorption from the moving bubble is described by the equation

$$U\frac{d}{dx}\left(\frac{4\pi}{3}r(x)^3 N_c\right) = -\pi\frac{4}{3}N_H D_H\left(\frac{3Ur(x)^3}{2\pi D_H}\right)^{0.5} \qquad (1)$$

Here x is a distance from the bottom of the BHP layer, r(x) is the bubble radius.

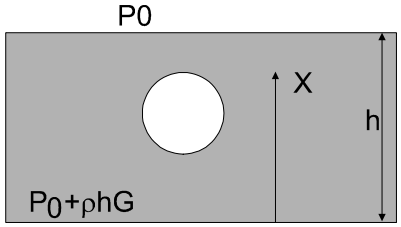

We will assume that pressure in the bubble approximately equals to pressure in an ambient BHP layer. Hence the radius of the bubble increases according to

$$r(x)^3 = P/P(x)r^3. \qquad (2)$$

where $P=P_0+\rho_l Gh$, $P(x)= P=P_0+\rho_l G(h-x)$. The residual chlorine partial concentration in the bubble is given by

$$N_c(x) = \frac{P(x)}{RT}\eta_c(x) \qquad (3)$$

where η_c is the molar fraction of the residual chlorine. The substitution of (2) and (3) gives equation for η_c

$$\frac{d\eta_c}{dx} = -\frac{N_H}{N_c}\left(\frac{3D_H}{2\pi r^3 U}\right)^{0.5}\left[\frac{P_0}{P_0 + \rho G(h-x)}\right]^{0.5} \qquad (4)$$

The solution of this equation gives the estimation of the chlorine utilization

$$Ut = 2\frac{N_H}{N_c}\left(\frac{3D_H}{2\pi r^3 U}\right)^{0.5}\left[\sqrt{\frac{P}{P_0}} - 1\right]\left(\frac{P}{P - P_0}\right) = \frac{h}{t_{ab}U}\left[\sqrt{\frac{P}{P_0}} - 1\right]\left(\frac{P}{P - P_0}\right) \qquad (5)$$

In this solution the bubble velocity was assumed constant.

Indeed $U=1.43(r(x)G)^{0.5}=1.43(rG)^{0.5}(P/P(x))^{1/6}$ and weakly depends on x. The formula (5) is valid when calculated Ut<1. The case Ut>>1 means that the flame sheet approximation is not valid and a surface reaction approximation have to be used. When Ut>1÷5, the absorption mode is intermediate between flame sheet approximation and surface reaction approximation. In this case it is necessary to compare values of times t_s, t_r.

Note to Item 12: The estimation of the detachment yield in the flame sheet model approximation is

$$Y_{det} \approx \frac{\alpha}{\alpha + \sqrt{\frac{D_o}{\tau_\Delta}}}\exp\left(-\frac{2N_c}{H_c N_H}\sqrt{\frac{\pi D_c t}{D_o \tau_\Delta}}\right), \qquad \frac{\alpha}{\alpha + \sqrt{\frac{\mathbf{D_o}}{\boldsymbol{\tau_\Delta}}}} \approx \mathbf{0.9}$$

where t is a time of starting of the BHP-Cl_2 contact. The most of the oxygen gas is produced near the bubble equator (t=r/U). Hence the estimation of the $O_2(^1\Delta)$ detachment yield is

$$Y_{det} \approx 0.9\exp\left(-\frac{2N_c}{H_c N_H}\sqrt{\frac{\pi D_c r}{U D_o \tau_\Delta}}\right)$$

Note to Item 13: $P\tau$ is defined as an average for pressure $(P + P_0)$ and divided by 2 because the $O_2(^1\Delta)$ is monotonically produced during time t_r.

Note to Item 14: It is assumed that distance between nozzles should be more than bubble diameter.

1.2. Estimation of RSSOG parameters for achieving P_0=100 torr.

A one example of the estimations of RSSOG parameters have been performed for the next a priory given input parameters and varied number of the revolutions per second:

Tab. 5

1	R=3 cm	Radius of RSSOG
2	d_0=0.02 cm=200 μm	Diameter of holes
3	H=0.3 cm	Height of BHP layer
4	w=0	Axial BHP velocity
5	n-varied	Revolutions per minute (RPM)
6	U_0=130 m/s	Gas velocity from nozzle
7	N_H=6 mole/L	BHP molarity (KOH)

The results of calculations according to the formula in Table 4 and for the input parameters in Table 5 are presented in **Figs. 1-5**. The dependences presented in Figures 1-5 can be explained qualitatively. When the centrifugal acceleration G is not too big the pressure P is close to P_0, and according to eq. (5), the utilization increases with increasing RPS. At higher G, the pressure P is substantially higher than P_0 and the chlorine concentration in the nozzle increases with increasing G. It explains non-monotonic dependence of the utilization, detachment yield and Pτ parameter with increasing RPS.

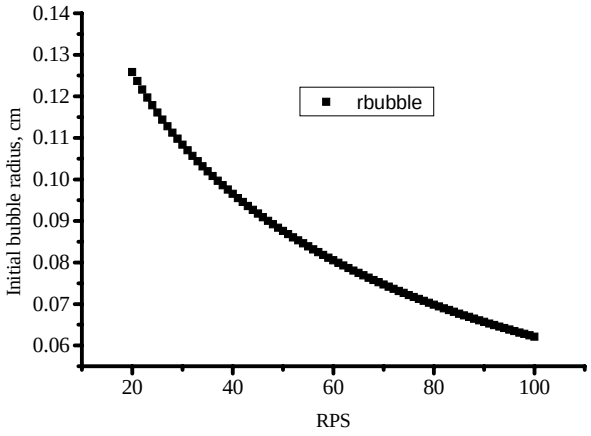

Fig. 1 The initial bubble radius as a function of the rotation rate (RPS)

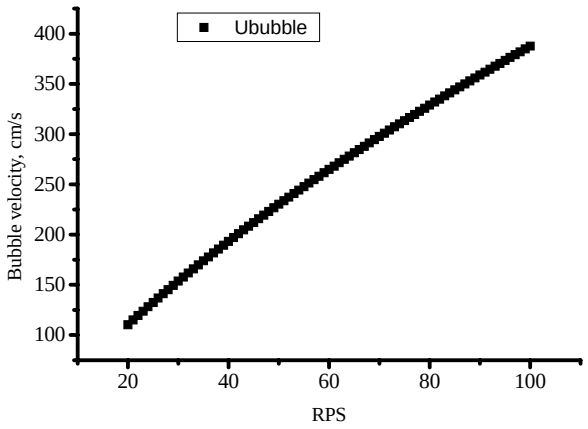

Fig. 2 Dependence of the bubble velocity on the number of RPS

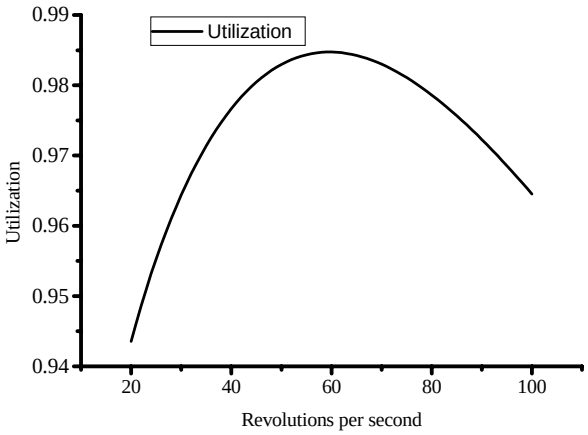

Fig. 3 Dependence of the chlorine utilization on RPS

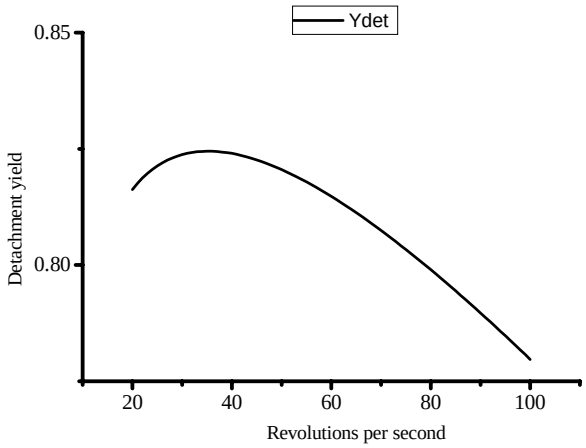

Fig. 4 Dependence of detachment $O_2(^1\Delta)$ yield (lower limit) on RPS

A lot of calculations have been performed. How the parameters indicated in Figs.1-5 are changed when other parameters in Table 5 are changed:

a) Nozzle diameter. A decrease in the nozzle diameter (lower than 200μm) results in a smaller bubble size, lower bubble velocity and higher utilization. However, simultaneously $P\tau$ increases and Y_{det} drops. It is necessary to decrease simultaneously the BHP layer height to maintain a high utilization and $O_2(^1\Delta)$ yield.

b) The gas velocity in the nozzles. An increase in the gas velocity results in increasing the bubble size and bubble velocity, which causes the utilization decrease. The maximum density of the nozzles in the bubbler decreases, the frequency of the bubble production decreases, and consequently the maximum oxygen flux doesn't increase substantially with increasing U_g.

c) The height of the BHP layer. With an increase in H, the utilization increases. However, increasing H results in the increase in the flight time t_f, and the increase in the bottom pressure P. This causes the Y_{det} drop and $P\tau$ increase.

d) The BHP molarity. The decrease in N_H substantially reduces the chlorine utilization and the detachment yield at a high initial chlorine pressure. To attain the required parameters with diluted BHP, it is necessary to decrease the nozzle diameter, gas velocity in the nozzle, the BHP height, and to increase the density of the nozzles.

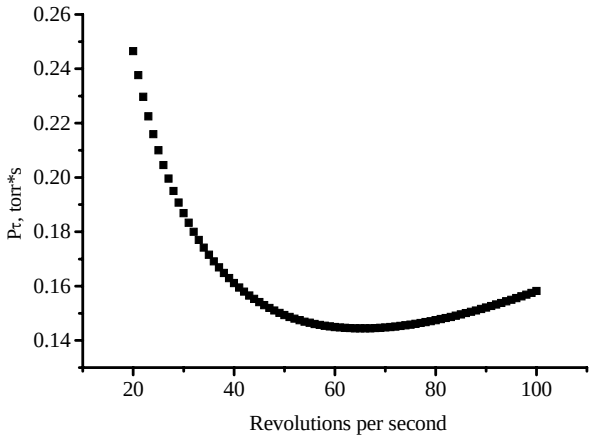

Fig. 5 Dependence of the quenching parameter Pτ on the RPS

Several sets of the parameters presented in Table 1 have been used in calculations. We select only those sets of the initial parameters, at which the required output parameters have been achieved. **Table 6** presents the estimation of other sets of the input parameters resulting in achieving a high utilization and $O_2(^1\Delta)$ yield of ~70% at the output pressure P_0=100 torr.

Tab. 6
The recommended initial RSSOG parameters for achievement of the high utilization and $O_2(^1\Delta)$ yield; the radius of the bubbler apparatus is R=3 cm

	Input parameters						Output parameters						
	n s^{-1}	H mm	d_0 μm	U_g m/s	N_H mole/L	w_r m/s	r mm	U cm/s	Ut	Y_{det}	Pτ torr×s	Y	M_c mmole/cm^2/s
1	60	3	200	130	6	11.1	0.8	250	~1	~80%	0.14	~0.7	~1
2	100	1.5	100	130	6	18.8	0.4	300	~1	~85%	0.08	~0.7	~1
3	80	6	300	130	6	9.4	0.9	3.8	~1	~70%	0.32	~0.5	~3
4	100	1	50	50	2	18.8	0.15	200	~1	~78%	0.06	~0.75	~0.5
5	80	1	50	100	3	9.4	0.2	200	~1	~80%	0.06	0.76	~0.5

Note: For all initial parameters $t_g<t_{ab}$ and $t_{dep}<<t_s$. Hence the flame sheet model approximation is valid.

The parameters in Table 6 correspond to only very rough estimation of RSSOG parameters. The main parameter for the COIL is the chlorine flux M_c or oxygen molar flow rate produced from 1 cm^2 of the bubbler layer. Parameterization showed that a high Y_{det}>80% and low Pτ<0.1 torr×s could be achieved at M_c≤1 mmole/cm^2/s, which is not enough large for the use in a COIL. The main reason is in requirement of the high pressure P_0=100 torr. The quenching of $O_2(^1\Delta)$ and depletion of HO_2^- in the

bubbler layer is very strong to ensure simultaneously a high utilization and Y>50% at M_c>1 mmole/cm^2/s and P_0=100 torr. Moreover, it is quite difficult to ensure good output parameters at the low BHP molarity. A higher $M_c \geq 3$ mmole/cm^2/s is possible to achieve at lower predicted yield $Y_{det} \leq 70\%$ and higher $P\tau > 0.2$ torr×s. So at higher M_c the predicted $O_2(^1\Delta)$ yield would be lower than 50%. It seems that the real liquid-gas hydrodynamic and mass transfer phenomena are much more complex. The heating of the BHP results in increasing in the mass transfer coefficients (D_c, D_H, D_o), the decrease in the BHP viscosity. These phenomena have to improve chlorine utilization. **The real output parameters of RSSOG can be much better at higher M_c. But only experiment can clear these problems and questions.**

1.3. Parameters of RSSOG at P_0<100 torr.

It was found that a decrease in the output pressure P_0 makes possible to increase the RSSOG specific output flux M_c and to save a high chlorine utilization and $O_2(^1\Delta)$ yield. Two sets of the input RSSOG parameters at P_0=20 torr are presented in **Table 6a**.

Tab. 6a
Example of the input-output parameters of the RSSOG at moderate P_0=20 torr

Input parameters						Output parameters					
	n s^{-1}	H mm	d_0 μm	U_g m/s	N_H mole/L	r mm	U cm/s	Ut	Y_{det}	Pτ torr×s	M_c mmole/cm^2/s
6	80	5	500	200	6	1.6	500	~1	>75%	0.16	~3
7	80	4	300	100	3	0.1	374	~1	70%	0.12	~2

2. Designing of parameters for the single pass burn down small-scale RSSOG ($M(O_2)$= 30 mmole/s, P_0=100 torr)

Additional specifications:

η_w – water vapour fraction

P_{wsi} – saturated water vapour pressure for the input BHP temperature T

P_{wsf} – saturated water vapour pressure for the output BHP temperature T_f

Y – expected $O_2(^1\Delta)$ yield

Z – axial length of the rotary bubbler

N_{Hf} – output concentration of the HO_2^- ions

t_{BHP} - BHP residence time in RSSOG

$M(O_2)$- output oxygen molar flow rate

In the single pass burn down RSSOG the output water vapour fraction should be enough low and the BHP consumption high. The estimations made below are based on the results present in the Report 001. We assume that the water fraction η_w=15% to the oxygen concentration does not decrease substantially the COIL gain and power in comparison with η_w=0. The fraction of the water vapour is given by ((24), Report 001):

$$\eta_w \approx\approx \frac{(1+A)P_{wsi}}{P_o}\frac{(P_{wsf}/P_{wsi})-1}{\ln\left(\frac{P_{wsf}}{P_{wsi}}\right)} \tag{6}$$

The water vapour partial pressure at input BHP temperature is given by

$$P_{wsi}(\text{torr}) = \exp\left(23.44-\frac{6051}{T}\right) \tag{7}$$

The water vapour partial pressure at output BHP temperature is given by

$$P_{wsf}(\text{torr}) = \exp\left(23.44-\frac{6051}{T_f}\right) \tag{8}$$

Assuming T=253K, dilution A=0, and P_0=100 torr, we obtain the required output BHP temperature $T_f \leq 315$K to maintain $\eta_w \leq 0.15$. The required maximum BHP residence time (t_{BHP}) in the RSSOG to ensure $T_f \leq 315$K and $\eta_w \leq 0.15$ is given by

$$t_{BHP} = \frac{Z}{W} = (T_f - T_i)\frac{HC_{BHP}}{M_c(Q_r + (1-Y)Q_\Delta)} \tag{9}$$

At maximum residence time (9) the output HO_2^- concentration is given by

$$N_{Hf} = N_H - \frac{2M_c}{H}t_{BHP} \tag{10}$$

In (9) and (10), $\mathbf{C}_{BHP}$=3.7 J/cm^3/K is the volume heat capacity of the BHP, Q_r =112×10^3 J/mole is the heat release in reaction $Cl_2+2HO_2^- \rightarrow 2Cl^-+H_2O+O_2(^1\Delta)$, Q_Δ=94×10^3 J/mole is the heat release in reaction $O_2(^1\Delta) \rightarrow O_2(^3\Sigma)$.

For the oxygen molar flow rate $M(O_2)$ and radius of the bubbler cylinder R=3 cm the, length Z of the perforated bubbler cylinder in the axial direction, the BHP axial velocity w and minimal volumetric rate V_{BHP} are correspondently equal to

$$Z = \frac{M(O_2)}{M_c 2\pi R} \tag{11}$$

$$w = \frac{Z}{t_{BHP}} = \frac{M(O_2)}{M_c 2\pi R t_{BHP}} \tag{12}$$

$$V_{BHP} = 2\pi RHw = H\frac{M(O_2)}{M_c t_{BHP}} = \frac{M(O_2)(Q_r + (1-Y)Q_\Delta)}{C_{BHP}(T_f - T_i)} \tag{13}$$

The minimal V_{BHP} depends only on required oxygen molar flow rate and on T_f (or P_0). If N_{Hf} defined by (10) is very low or less than 0 the BHP volumetric rate should be higher than defined from water vapour management (13). We will suppose in this case that the BHP residence time should be short enough to support $N_{Hf} \geq N_H/2$ and good chlorine absorption conditions. Hence the maximum BHP residence time is in this case

$$t_{BHP} = (N_H / 4)(H / M_c) \qquad (14)$$

For RSSOG parameters in Tables 6 and 6a, we obtain the required BHP residence time in RSSOG, consumption of BHP alkaline molarity, the axial length, axial velocity and volumetric rate of the BHP. Hence the final designing parameters and expected output parameters are presented in **Table 7**.

Tab. 7
The preliminary designing parameters and expected output parameters for M(O2)=30 mmole/s (explanation in Fig.6)

Input parameters (T=253K, P_0=100 torr, Table 6)							Output parameters (T_f=315K, $\eta_w \leq 0.15$)				
Item	n s^{-1}	H mm	d_0 μm	U_g m/s	N_H mole/L	M_c mmole/cm^2/s	t_{BHP},s	Z cm	w cm/s	V_{BHP} L/s	N_{Hf} mole/L
1	60	3	200	130	6	~1	0.5	1.6	3.2	0.018	2.7
2	100	1.5	100	130	6	~1	0.25	1.6	6.4	0.018	2.7
In Items 3-4 the BHP volumetric flow rate should be higher than defined from (13) or t_{BHP} should be defined from (14) to keep $N_{Hf} > N_H/2$ mole/litre											
3	80	6	300	130	6	~3	0.3	0.53	1.8	0.02	3
4	80	1	50	100	3	~0.5	0.15	3.2	21.3	0.04	1.5
5	100	1	50	50	2	~0.5	0.1	3.2	32	0.06	1
Input parameters for the moderate pressure RSSOG (T=253K, P_0=20 torr, Table 6a)							Output parameters (T_f=284K, $\eta_w \leq 0.15$).				
6	80	5	500	200	6	~3	0.14	0.53	3.8	0.036	4.3
7	80	4	300	100	3	~2	0.1	0.8	8	0.06	2

The efficiency of the BHP consumption at high P_0 is close to 50%. At moderate pressure P_0=20 torr the consumption of the BHP is lower. The most suitable input parameters are in Item 3 at P_0=100 torr and Item 6 for P_0=20 torr.

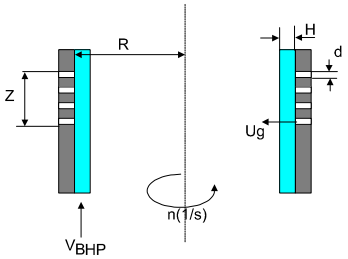

Fig. 6 Designing parameters of RSSOG

3. Principle constructions of the small-scale RSSOG for production of 30 mmole/s of oxygen flow (close coupling of the generator to nozzle plenum to minimize $O_2(^1\Delta)$ loss and disengagement of gas/liquid)

The volumetric rate of the gas over BHP bubbler layer is

$$V_{gas} = \frac{M(O2)RT}{P_0} \qquad (15)$$

R_g=8.31 J/mole/K is the universal gas constant. The gas transport time from the BHP bubbler layer to the throat of the nozzle bank is equal to

$$t_{trans} = \frac{V_0}{V_{gas}} = \frac{V_0 P_0}{M(O2)R_g T}, \qquad (16)$$

V_0 is the volume of the transport duct between the BHP surface and the nozzle throat.

The so-called quenching parameter Pτ due to reactions $O_2(^1\Delta)+O_2(^1\Delta)\rightarrow O_2(^1\Sigma) +O_2(^3\Sigma)$ is equal to

$$P_0 t_{trans} = \frac{P_0 V_0}{V_{gas}} = \frac{V_0 P_0^2}{M(O2)R_g T} \qquad (17)$$

Let's require $(P_0 t_{trans}) < \chi_{max}$ =0.1 torr×s. Hence the maximum volume of the transport duck

$$V_0 < \frac{\chi_{max}}{P_0}\frac{M(O2)}{P_0}R_g T \qquad (18)$$

For the input parameters presented in Table 7, the maximum volumes of the transport duct between the bubbler BHP layer and the nozzle throat are presented in **Table 8**.

Tab. 8

(Items 1-7 are the same like in Tables 6 and 6a)

	Output pressure P_0, torr	Axial length of RSSOG Z, cm	Chlorine flux through bubbler surface M_c mmole/cm^2/s	Required maximum volume of transport duct from BHP surface to nozzle throat V_0, cm^3
1	100	1.6	1	4.8
2	100	1.6	1	4.8
3	100	0.53	3	4.8
4	100	3.2	0.5	4.8
5	100	3.2	0.5	4.8
6	20	0.53	3	120
7	20	0.8	2	120

Table 8 shows that the required transport duct volume is too small for Items 1-5. It is quite difficult to imagine an assembling of RSSOG with R=3 cm and Z≈1 cm, and with the nozzle bank keeping the plenum pressure P_0=100 torr and keeping $O_2(^1\Delta)$ yield (Items 1-5).

Much more promising is the scheme of COIL with output oxygen pressure P_0=20 torr (Items 6-7). Also the COIL schemes with RSSOG parameters according to Items (1-5) with output pressure P_0=100 torr can be realized using oxygen pressure discharge from the output pressure P_0=100 torr to the plenum pressure P_{plen}=20 torr. The discharge of the pressure can be realized immediately after oxygen outlet from BHP. In this case the required maximum transport volume is equal to 120 cm^3 (like for items 6-7) and large enough for the arrangement of the nozzle bank.

Scheme 1

The principle scheme of RSSOG with output and plenum oxygen pressure 20 torr is presented in **Fig.7**. The RSSOG can be scaled in Z and R directions. The appropriate changes of parameters w, V_{BHP} should be made according to formulas (11)-(14). For example, increasing Z twice forces an increase in the axial velocity w and the BHP volumetric rate twice. The principle assembling of three or several RSSOG is presented in **Fig.8**.

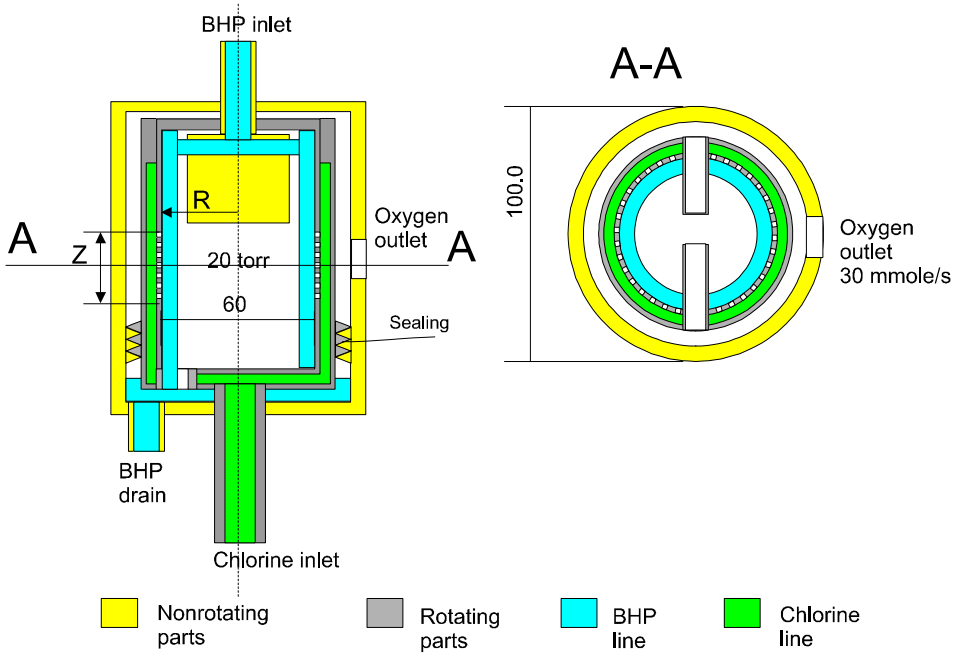

Fig. 7 Principle scheme of RSSOG

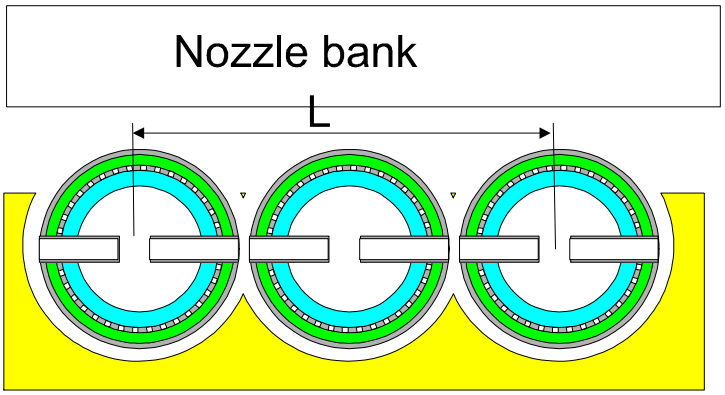

Fig. 8 Principle of several RSSOG assembling

Let's present some technical characteristics of the assembling of several RSSOG. The oxygen plenum flux (in front of the nozzle bank) is $M_{O2}=nM_c2\pi R/L$, where n is the number of RSSOG, L is the length of assembling on n RSSOG. For $M_c=3$ (mmole/s)/cm^2 the oxygen plenum flux of the order of 7 (mmole/s)/cm^2 can be generated by this set of small scale RSSOG. The ratio of the total oxygen molar flow rate to the BHP volumetric rate of the order of 1.5 (mole/s)/(litre/s) for Item 3 and 0.8 (mole/s)/(litre/s) for Item 6 can be achieved.

Scheme 2

The principle scheme with output pressure 100 torr and plenum pressure 20 torr is presented in **Fig. 9** and is similar to the scheme in Fig. 8 with the difference that a perforated wall is installed over the BHP surface to discharge the oxygen pressure from 100 torr to 20 torr.

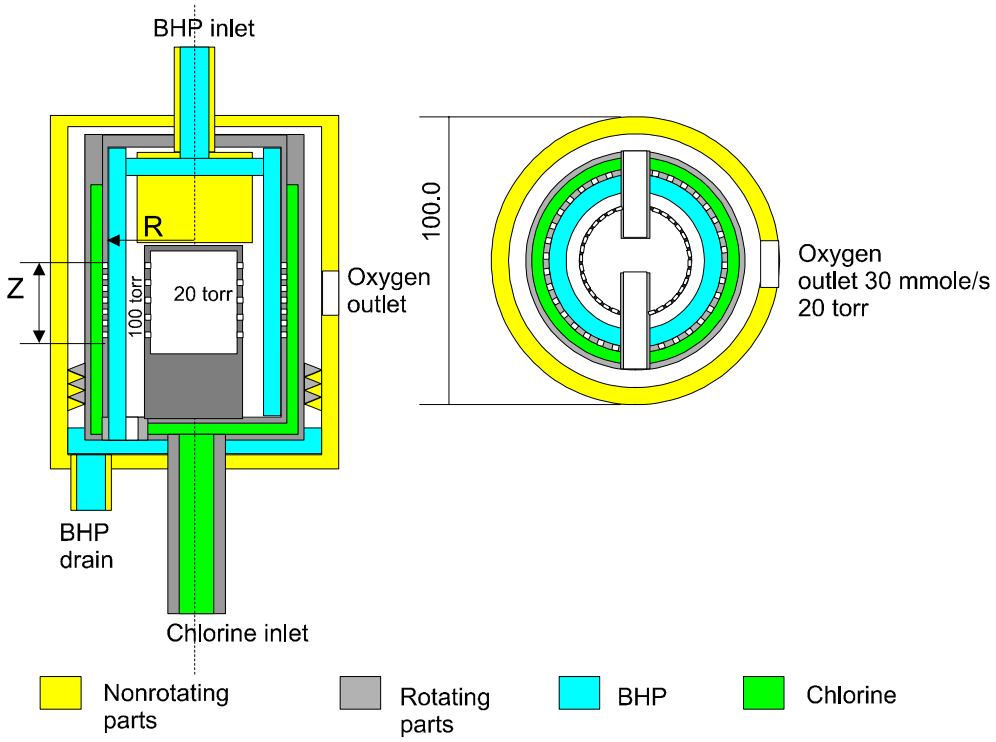

Fig. 9 Principle scheme of RSSOG with oxygen pressure discharge

Scheme 3

The assembling of several RSSOG in vertical Z direction is presented in **Fig. 10**. In this scheme, the length Z is of the order of several cm and axial velocity w of the order of several ten centimetres per second. The worked-out BHP drains to the common collector.

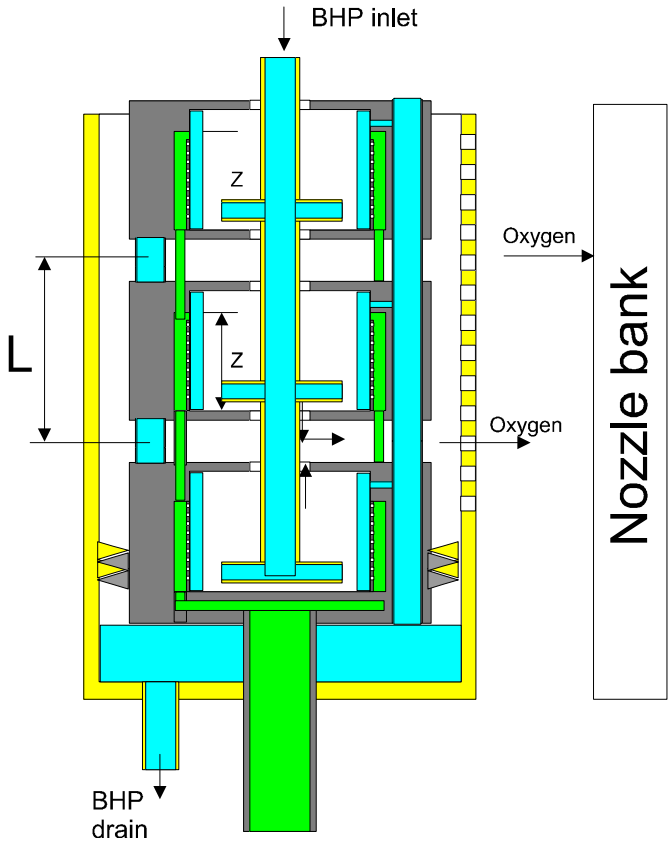

Fig. 10 Principle scheme of RSSOG with vertical scaling

4. Conclusions

The conception of the centrifugal bubble SOG is based on understanding that the mass transfer phenomena for these conditions are much faster than in any another type mass-transfer apparatus. Hence very efficient production of the oxygen flow with high $O_2(^1\Delta)$ yield and chlorine utilization is possible. The estimation of the gas-liquid hydrodynamic of centrifugal bubble SOG is based on the literature data reviewed in Report 001 of this grant. The estimation of chlorine utilization and $O_2(^1\Delta)$ production is based on the modern understanding of the mass-transfer phenomena in the chlorine-BHP system. Nevertheless, we understand that all estimations are very rough because the real hydrodynamics and the mass-transfer processes in the centrifugal bubbler SOG are much more complex. Very simplified model of the processes described above gives a very approximate parameters of RSSOG to achieve required output parameters and suitable for COIL application. According to these estimations, the oxygen flux M_{O2}~3 (mmole/s) per 1 cm^2 of the bubbler surface can be produced at the output oxygen pressures 20÷100 torr. A possible production of higher oxygen flux (with high $O_2(^1\Delta)$ yield, high utilization and pressure >20 torr) is a question. For M_{O2}<3 mmole/s and high P_0, the transport volume duct between RSSOG and the nozzle ban (NB) should be very small to save $O_2(^1\Delta)$, so it is quite difficult to invent efficient RSSOG + nozzle bank system. The discharge of oxygen plenum pressure to 20 torr would make possible to solve the problem of oxygen transport from the RSSOG to the NB. Using of diluted BHP with low KOH (NaOH, LiOH) concentration substantially decreases the efficiency of chlorine utilization and very hardly designed parameters of RSSOR (a small nozzle diameter, a high centrifugal acceleration) are required. Several schemes of RSSOG and scaling procedures are proposed in this Report. The RSSOG can work in the single pass burn down with efficient BHP consumption. The predicted ratio of chlorine molar flow rate to BHP volumetric rate is of the order of 1(mole/s)/(litre/s) in the single pass burn down mode. This ratio is much higher than for another SOG types. The scaling of RSSOG is evident and clear. A plenum oxygen flux in front of the large scale NB of the order of 7 mmole/cm^2/s can be produced by assembling several RSSOG.

B. Concept(s) investigated in the COIL Laboratory in Prague

Two concepts of the advanced generator of singlet oxygen were proposed employing a centrifugal force for gas/liquid disengagement: the Centrifugal Film SOG (CentFilmSOG) and Centrifugal Spray SOG (CentSpraySOG). They were described in the interim Report 001 submitted to the EOARD on 31 July 2004. Theoretical estimations of both concepts showed that the CentSpraySOG would better fulfill requirements given in Objects and Goals of this investigation, and therefore, our recent research has been focused on more detailed computational modeling of parameters of this generator, and designing devices for its experimental investigation.

Centrifugal Spray Singlet Oxygen Generator (CentSpraySOG)

This concept is based on principle of the efficient generation of singlet oxygen in mixture of chlorine and BHP spray (mist), from which liquid droplets are efficiently separated by a centrifugal force within very short time. The mist of small-diameter droplets of tens microns provides a large specific surface area and a short diffusion path of HO_2^- ions from the bulk BHP, resulting in substantially better BHP utilization than in any other types of chemical generators (jet-type, disk-type). Calculations performed at the USAF by Blauer, et al. [1] on the aerosol generator showed that the generator operating at moderate $O_2(^1\Delta)$ pressures (~20 Torr) and with a high $O_2(^1\Delta)$ yield (~70%) may be designed with very restrictive dimensions to limit a time of the two-phase flow below a few milliseconds. Our new proposed concept of CentSpraySOG employing a combination of the spray SOG and centrifugal separator of both phases may overcome this problem.

1. Principle design and operation of CentSpraySOG

The proposed concept is schematically shown in **Fig. 1**. Operation of the device can be simply described by the following processes:

- An atomizing nozzle (**Fig. 2**) produces a spray (mist) of BHP droplets by means of pressurized Cl_2/He (N_2) gas mixture.
- Droplets of partially exhausted BHP are separated from g/l mixture by a centrifugal force of the rotating blade separator within a few milliseconds (**Fig. 3**).

- A liquid-free gas (containing $O_2(^1\Delta)$, residual Cl_2, buffer gas and residual water vapor) leaves the generator through the exit coupled to the laser nozzle throat, while the liquid is collected in the bottom tank.

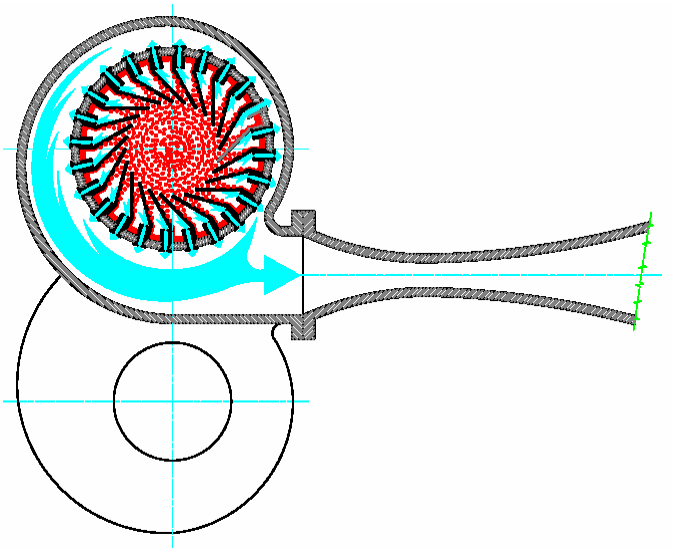

Fig. 1 Scheme of principle of CentSpraySOG device

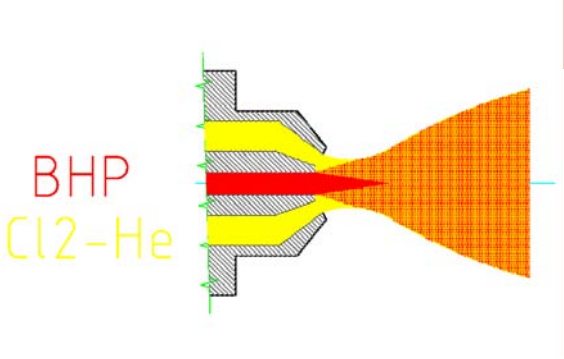

Fig. 2 Scheme of two-phase spray nozzle

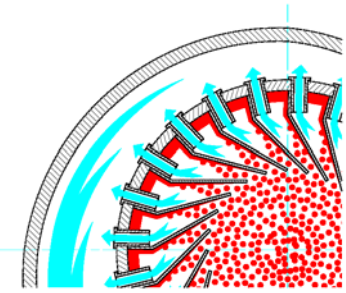

Fig. 3 Scheme of centrifugal separator

2. Estimation of main characteristics of the spray SOG

Parametric estimation of the spray generator was performed for conditions listed in **Table 1.**

Tab. 1
Main parameters of the reaction system

Characteristics	Labeling	Magnitude
Gas entering the generator	Cl_2 + He	1 : 4
Total generator pressure	P_{tot}	40 kPa (300 torr)
Gas temperature	T	260 K
BHP droplet radius	a	10 μm
Diffusion coefficient of chlorine in gas	D_{CG}	3.3×10^{-5} m^2 s^{-1}
Diffusion coefficient of chlorine in BHP	D_{CL}	5×10^{-10} m^2 s^{-1}
Diffusion coefficient of HO_2^- in BHP	D_{HL}	5×10^{-10} m^2 s^{-1}
Diffusion coefficient of oxygen in BHP	$D_{\Delta L}$	5×10^{-10} m^2 s^{-1}
Initial HO_2^- concentration in BHP	c_{HL0}	5 kmol m^{-3}
Initial Cl_2 concentration in gas	c_{CG0}	3.7×10^{-3} kmol m^{-3}
Rate constant of reaction $Cl_2 + HO_2^-$	k_p	5×10^8 m^3 kmol^{-1}s^{-1}
Striking Cl_2 probability at BHP surface	γ_C	0.0075
Striking $O_2(^1\Delta_g)$ probability at BHP surface	γ_Δ	0.003
Henry constant of chlorine	H_C	1
$O_2(^1\Delta_g)$ lifetime in BHP	τ_Δ	2×10^{-6} s
Rate constant of $O_2(^1\Delta_g)$ dimolar reactions in (g)	k_{QG}	3.7×10^4 m^3 kmol^{-1}s^{-1}

The calculations of characteristic times of partial steps in the whole process, i.e., the characteristic time of HO_2^- depletion in droplet controlled by interfacial crossing or reactive diffusion in liquid, the characteristic time of Cl_2 depletion, the estimation of $O_2(^1\Delta)$ detachment yield and $O_2(^1\Delta)$ loss in the gas phase, were presented in detail in the interim report of this grant. Below are summarized therefore only **conclusions from these estimations.**

- The process of $O_2(^1\Delta_g)$ generation in the proposed conditions is controlled first by chlorine absorption (interfacial crossing) (t < 0.3 ms).
- After this first period, the process is controlled by HO_2^- diffusion from the droplet interior.
- Chlorine is nearly exhausted within 3 ms.
- ~ 40 % of HO_2^- ions of BHP is consumed within this time.
- The $O_2(^1\Delta_g)$ yield at the generator exit decreases with time from 0.73 (after 1 ms) to 0.50 (after 4 ms).

3. Detailed theoretical description of CentSpraySOG

Tab. 2
List of main symbols

a	Radius of droplet
b	Radius of gas volume surrounding the droplet
c_{if} $(i=C,H,\Delta;f=G,L)$	Molar concentration of HO_2^-, Cl_2, and $O_2(^1\Delta)$ in gas and liquid phase
c_{isG}, c_{isL}	Molar concentration at the g/l interface on the gas or liquid side
c_{HL0}, c_{CG0}	Initial (bulk) concentration of HO_2^- and Cl_2
$\bar{c}_{CG}$, $\bar{c}_{\Delta G}$	Averaged concentration of Cl_2 and $O_2(^1\Delta)$ in the gas phase
D_{if} $(i=C,H,\Delta;f=G,L)$	Diffusion coefficient of species in gas or liquid phase
t	Time since droplets escaped from the nozzle
$H_i = (c_{iG}/c_{iL})_{eq}$	Dimensionless Henry constant of species i
$\alpha_i = 1/4 v_{t,i}\gamma_i$	Mass transfer coefficient of species i across g/l interface
γ_i	Stricking probability of species i
$v_{t,i}$	Thermal velocity of species i
r	Radial coordinate from the center of droplet
U_i	Utilization

A volumetric fraction of the liquid in the aerosol can be expressed as

$$\lambda = \left(1 + \frac{u}{2}\frac{c_{HL0}}{c_{CG0}}\right)^{-1}, \qquad (1)$$

where $u \equiv U_H / U_C$. If the process runs for an infinitely long time the ultimate concentrations for the case of initial stoichiometry, i.e.

$$2\ V_G\ c_{CG0} = V_L\ c_{HL0} \qquad (2)$$

for $u < 1$ would be

$$c_{HL\infty} = (1-u)c_{HL0}, \quad c_{CG\infty} = 0, \qquad (3)$$

and for $u > 1$: $c_{HL\infty} = 0$, $c_{CG\infty} = (1-1/u)c_{CG0}$. (4)

3.1. Mass transfer in liquid phase

A temporal profile of the HO_2^- concentration in the liquid can be considered for two limiting cases.

3.1.1. Initial (film) stage

In the initial stage, the diffusion-reaction kinetics is limited by molecular transport at the interface. It can be assumed that the flux of HO_2^- towards the phase interface is constant in time. The corresponding solution is then (adaptation of eq. 1 in [2], p. 242)

$$c_{HL} = c_{HL0} - j_H\left[\frac{3t}{a} + \frac{5r^2 - 3a^2}{10D_H a} - \frac{2a^2}{D_H r}\sum_{n=1}^{\infty}\frac{\sin(r\alpha_n / a)}{\alpha_n{}^2 \sin\alpha_n}\exp\left(-\frac{D_H \alpha_n{}^2 t}{a^2}\right)\right] \quad (5)$$

where α_n, $n = 1,2,\ldots$, are the positive roots of

$$\tan\alpha = \alpha, \quad \text{or} \quad \alpha\cos\alpha - \sin\alpha = 0, \quad (6)$$

and j_H is the molar flux of HO_2^-.

The first root of eq. (6) is $\alpha_i = 4.4934$. Higher roots were found using the Newton-Raphson method with $\alpha_n^{(0)} = \alpha_{n-1} + \pi$. The iteration of more general form of this equation will be discussed later.

Using dimensionless variables $y \equiv r/a$ and $\tau \equiv tD_H / a^2$, eq. (5) can be written as

$$c_{HL} = c_{HL0}\left(1 - \phi_H\left[3\tau + \frac{5y^2 - 3}{10} - \frac{2}{y}\sum_{n=1}^{\infty}\frac{\sin(\alpha_n y)}{\alpha_n^2 \sin\alpha_n}\exp(-\alpha_n^2\tau)\right]\right), \quad (7)$$

where

$$\phi_H = \frac{j_H a}{D_H c_{H0}}. \quad (8)$$

The surface concentration (y=1) is

$$c_{HsL} = c_{HL0}\left(1 - \phi_H\left[3\tau + \frac{1}{5} - 2\sum_{n=1}^{\infty}\frac{1}{\alpha_n^2}\exp(-\alpha_n^2\tau)\right]\right) \equiv c_{HL0}[1 - \phi_H \vartheta_{Hs}(\tau)] \quad (9)$$

The significance of the sum of exponentials decreases sharply with growing τ. For $\tau = 0.1$ it contributes less than 3%.

The mean concentration averaged from $r = 0$ to $r = a$ is

$$\bar{c}_{HL} = \frac{\int_0^a c_{HL} 4\pi r^2 dr}{\frac{4}{3}\pi a^3} = c_{HL0} - \frac{3 j_H t}{a}. \quad (10)$$

If $\sqrt{D_H t} << a$, the influence of curvature can be neglected and the case can be treated as diffusion into a semi-infinite solid (adapt. eq. 7 in [2], p. 75):

$$c_{HL} = c_{HL0} - \frac{2 j_H}{D_H}\left[\sqrt{\frac{D_H t}{\pi}}\exp\left(-\frac{x^2}{4D_H t}\right) - \frac{x}{2}erfc\left(\frac{x}{2\sqrt{D_H t}}\right)\right], \quad (11)$$

where $x \equiv a - r$ and

$$erfc \equiv \frac{2}{\sqrt{\pi}}\int_x^{\infty} e^{-\xi^2} d\xi. \quad (12)$$

3.1.2. Final (depleted surface) stage

In the final stage, the diffusion-reaction kinetics is limited by the transport of HO_2^- towards the phase interface. We assume $c_{HsL} << \bar{c}_{HL}$, which allows an approximation $c_{HsL} \approx 0$. An adaptation of eq. 4 in [2], p. 233 gives

$$c_{HL} = -c_{HL0}\frac{2a}{\pi r}\sum_{n=1}^{\infty}\frac{(-1)^n}{n}\sin\frac{n\pi r}{a}\exp\left(-\frac{D_H n^2\pi^2 t}{a^2}\right). \quad (13)$$

The average concentration at time t is given as (adapt. of eq. 8. in [2], p. 234)

$$\bar{c}_{HL} = c_{HL0}\frac{6}{\pi^2}\sum_{n=1}^{\infty}\frac{1}{n^2}\exp\left(-\frac{D_H n^2\pi^2 t}{a^2}\right). \quad (14)$$

The flux at the surface ($r = a$) is given as

$$j_H = -D_H\frac{\partial c_{HL}}{\partial x} = \frac{D_H c_{HL0}}{a}2\sum_{n=1}^{\infty}\exp\left(-\frac{D_H n^2\pi^2 t}{a^2}\right). \quad (15)$$

3.1.3. Matching the initial and final solution

An approximation for the diffusion kinetics in the whole domain can be obtained by combining the initial and final solutions. The initial and final solutions are matching at the time t_d, for which two conditions are satisfied: (i) the fluxes are equal, and (ii) the mean concentrations are equal. In order to achieve that solution, a start of the final solution is postponed by a time interval $\Delta t, (\Delta t < t_d)$. Parameters t_d and Δt are adjusted to satisfy the above two conditions.

The computation is done as follows. We assume that the initial flux is given, and then the dimensionless form can be used

$$\phi_{H,ini} = \frac{j_{H,ini}a}{D_H c_{HL0}}. \quad (16)$$

The mean concentration from the initial solution at the matching point is

$$\bar{c}_{HL,ini,d} = c_{HL0}\left(1-\frac{3D_H t_d}{a^2}\phi_{H,ini}\right), \quad (17)$$

and the dimensionless flux computed from the final solution is given as

$$\phi_{H,fin,d} = \frac{j_{H,fin,d}a}{D_H c_{HL0}} = 2\sum_{n=1}^{\infty}\exp\left[-n^2\pi^2\frac{D_H}{a^2}(t_d-\Delta t)\right]. \quad (18)$$

By setting $\phi_{H,fin,d} = \phi_{H,ini,d}$, eq. (17) can be iterated to obtain $(t_d - \Delta t)$. The mean concentration at the matching point, computed from the initial solution, is given as

$$\bar{c}_{HL,fin,d} = c_{HL0}\frac{6}{\pi^2}\sum_{n=1}^{\infty}\frac{1}{n^2}\exp\left[-n^2\pi^2\frac{D_H}{a^2}(t_d-\Delta t)\right] = c_{H,0}\vartheta_{fin}(t_d-\Delta t). \quad (19)$$

The right-hand side can be evaluated because $(t_d - \Delta t)$ is already known.

By setting $\bar{c}_{H,fin,d} = \bar{c}_{H,ini,d}$, we then have

$$t_d = a^2 \frac{1-\vartheta_{fin}(t_d - \Delta t)}{3D_H \phi_{H,ini}} \quad . \tag{20}$$

The delay time is then obtained as $\Delta t = t_d - (t_d - \Delta t)$.

3.2. Mass transport at g/l interface

3.2.1. Transport across the interface

It is assumed that temperature at both sides of the phase interface is the same. The net flux of the species *i* from the gas phase to the liquid phase is

$$j_{is} = \alpha_i (c_{isG} - c^E_{IsG}) = 1/4 \gamma_i v_{t,i} (c_{isG} - H_i c_{isL}) . \tag{21}$$

3.2.2. Diffusion-reaction kinetics of Cl_2

We use here the coordinate $x \equiv r - a$. The diffusion-reaction equation is

$$\frac{\partial c_{CL}}{\partial t} = D_{CL} \frac{\partial^2{}_{CL}}{\partial x^2} - k_P c_{HL} c_{CL} \approx 0 . \tag{22}$$

Solution of this equation can be found when approximating $c_{HL}(x) \approx c_{HsL}$ (i.e. the concentration variation of HO_2^- is much smaller then of Cl_2)

$$c_{CL} = c_{CsL} \exp \frac{x}{X_P} , \tag{23}$$

where

$$X_P = \sqrt{\frac{D_{CL}}{k_P c_{HsL}}} . \tag{24}$$

The flux of Cl_2 is given by

$$j_{CL} = -D_{CL} \frac{\partial c_{CL}}{\partial x} = -D_{CL} \frac{c_{CsL}}{X_P} \exp \frac{x}{X_P} = -c_{CsL} \sqrt{D_{CL} k_P c_{HsL}} \exp \frac{x}{X_P} \quad , \tag{25}$$

and at the surface

$$j_{CsL} = -D_{CL} \frac{c_{Csl}}{X_P} = -c_{CsL} \sqrt{D_{CL} k_P c_{HsL}} . \tag{26}$$

Combining the equations (26) and (21), we obtain

$$j_{Cs} = -\frac{\alpha_C c_{CsG}}{1 + \alpha_C H_C X_P / D_{CL}} . \tag{27}$$

3.2.3. Diffusion-reaction kinetics of $O_2(^1\Delta)$

The second Fick's law for singlet oxygen has the form

$$\frac{\partial c_{\Delta L}}{\partial t} = D_{\Delta L} \frac{\partial^2{}_{\Delta L}}{\partial x} + k_P c_{HL} c_{CL} - k_{QL} c_{\Delta L} , \tag{28}$$

In the steady state, the left side of this equation is nearly zero.

Using (23), setting $c_{HL}(x) \approx c_{HsL}$, and the condition of $c_{\Delta L}(x \to \infty) = 0$, we can finally obtain by integration (28)

$$c_{\Delta L} = c_{CsL}\chi \exp(x / X_P) + (c_{\Delta sL} - c_{CsL}\chi)\exp(x / X_{QL}), \tag{29}$$

where

$$X_{QL} = \sqrt{D_{\Delta L} / k_{QL}}, \tag{30}$$

$$\chi = \frac{D_{CL}}{D_{\Delta L}}\left[\left(X_P / X_{QL}\right)^2 - 1\right]^{-1}. \tag{31}$$

The corresponding flux of $O_2(^1\Delta)$ is

$$j_{\Delta L} = -D_{\Delta L}\frac{\partial c_\Delta}{\partial x} = -D_{\Delta L}\left(\frac{c_{CsL}\chi}{X_P}\exp\frac{x}{X_P} + \frac{c_{\Delta sL} - c_{CsL}\chi}{X_{QL}}\exp\frac{x}{X_{QL}}\right). \tag{32}$$

Especially for the phase interface $(x = 0)$, the flux is then

$$j_{\Delta sL} = D_{CL}c_{CsL}\frac{1}{X_P}\frac{1}{1 + X_P / X_{QL}} - D_{\Delta L}c_{\Delta sL}\frac{1}{X_{QL}}. \tag{33}$$

and

$$j_{\Delta sL} = -\alpha_\Delta(c_{\Delta sG} - H_\Delta c_{\Delta sL}). \tag{34}$$

By combining eqs. (33) and (34), we obtain

$$j_{\Delta s} = \frac{\left(\frac{D_{Cl}c_{CsL}}{X_P}\frac{1}{1 + X_P / X_{QL}} - \frac{D_{\Delta L}c_{\Delta sG}}{X_{QL}H_\Delta}\right)}{\left(1 + \frac{X_\Delta}{X_{QL}}\right)}, \tag{35}$$

where

$$X_\Delta = \frac{D_{\Delta L}}{\alpha_\Delta H_\Delta} \tag{36}$$

The length X_Δ can be interpreted as a thickness of hypothetical additional layer of liquid, through which $O_2(^1\Delta)$ must diffuse.

Using eq. (35)

$$j_{\Delta s} = \frac{\left(-\frac{j_{CsL}}{1 + X_P / X_{QL}} - \frac{D_{\Delta L}c_{\Delta sG}}{X_{QL}H_\Delta}\right)}{\left(1 + \frac{X_\Delta}{X_{QL}}\right)}. \tag{37}$$

3.2.4. Simplified evolution equations for Cl_2 and $O_2(^1\Delta)$ concentrations in gas

Because the diffusion of Cl_2 and $O_2(^1\Delta)$ in the gas phase is fast in comparison with the HO_2^- diffusion in the liquid, it is possible to ignore the spatial gradient of their concentrations:

$$\bar{c}_{CG} \approx c_{CsG},$$
$$\bar{c}_{\Delta G} \approx c_{\Delta sG}. \tag{38}$$

Then the evolution of chlorine concentration is given as

$$\frac{4}{3}\pi(b^3-a^3)\frac{d\bar{c}_{CG}}{dt}=4\pi a^2 j_{Cs}, \tag{39}$$

$$\frac{d\bar{c}_{CG}}{dt}=\frac{1}{a}\frac{3\lambda}{1-\lambda}j_{Cs}. \tag{40}$$

It follows from the stoichiometry that

$$\bar{c}_{CG}(t)=c_{CG0}+\frac{\dot{V}_L}{2\dot{V}_G}[\bar{c}_{HL}(t)-c_{HL0}]=c_{CG0}+\frac{\lambda}{2(1-\lambda)}[\bar{c}_{HL}(t)-c_{HL0}]. \tag{41}$$

The evolution of $O_2(^1\Delta)$ concentration is given as

$$\frac{4}{3}\pi(b^3-a^3)\frac{d\bar{c}_{\Delta G}}{dt}=4\pi a^2 j_{\Delta s}=\frac{4}{3}\pi(b^3-a^3)k_{QG}\bar{c}^{\,2}{}_{\Delta G}, \tag{42}$$

$$\frac{d\bar{c}_{\Delta G}}{dt}=\frac{1}{a}\frac{3\lambda}{1-\lambda}j_{\Delta s}-k_{QG}\bar{c}^{\,2}{}_{\Delta G}. \tag{43}$$

For constant flux j_Δ and initial condition $c_{\Delta G}(t=0)=0$ the equation (43) can be integrated:

$$\bar{c}_{\Delta G}(t)=\frac{1}{k_{QG}t_\Delta}\tanh\frac{t}{t_\Delta}, \tag{44}$$

where the characteristic time is $$t_\Delta\equiv\sqrt{\frac{(1-\lambda)a}{3\lambda j_{\Delta s}k_{QG}}}. \tag{45}$$

Using eq. (43) and (37), we obtain

$$\frac{d\bar{c}_{\Delta G}}{dt}=\frac{1}{a}\frac{3\lambda}{1-\lambda}\frac{\left(-\dfrac{j_{CsL}}{1+X_P/X_{QL}}-\dfrac{D_{\Delta L}c_{\Delta sG}}{X_{QL}H_\Delta}\right)}{\left(1+\dfrac{X_\Delta}{X_{QL}}\right)}-k_{QG}\bar{c}^{\,2}_{\Delta G}. \tag{46}$$

The last equation can be written as

$$\frac{\partial\bar{c}_{\Delta G}}{\partial t}=q_P+q_{QL}+q_{GQ}, \tag{47}$$

where $$q_P=\frac{1}{a}\frac{3\lambda}{1-\lambda}\frac{-\dfrac{j_{CsL}}{1+X_P/X_{QL}}}{\left(1+\dfrac{X_\Delta}{X_{QL}}\right)}, \tag{48}$$

$$q_{QL}=\frac{1}{a}\frac{3\lambda}{1-\lambda}\frac{\dfrac{D_{\Delta L}c_{\Delta sG}}{X_{QL}H_\Delta}}{\left(1+\dfrac{X_\Delta}{X_{QL}}\right)}, \tag{49}$$

$$q_{QG} \equiv -k_{QG}\bar{c}_{\Delta G}^{2}. \quad (50)$$

After formal integration, $$\bar{c}_{QG} = Q_P + Q_{QL} + Q_{QG}, \quad (51)$$

where $$Q_i = \int_0^t q_i(t')dt'. \quad (52)$$

4. Numerical solution of generator parameters

Differential equations described in the chapter 3 were solved numerically for general parameters listed in **Table 3**.

Tab. 3

Characteristics	**Label**	**Magnitude**
Diffusion coefficient of chlorine in BHP	D_{CL}	5×10^{-10} m^2 s^{-1}
Diffusion coefficient of HO_2^- in BHP	D_{HL}	5×10^{-10} m^2 s^{-1}
Diffusion coefficient of oxygen in BHP	$D_{\Delta L}$	5×10^{-10} m^2 s^{-1}
Rate constant of reaction $Cl_2 + HO_2^-$	k_p	5×10^8 m^{3}kmol^{-1}s^{-1}
Sticking probability of Cl_2 at BHP surface	γ_C	0.0075
Sticking probability of $O_2(^1\Delta_g)$ at BHP surface	γ_Δ	0.003
Henry constant of chlorine	H_C	1
Henry constant of oxygen	H_O	20
$O_2(^1\Delta_g)$ lifetime in BHP	τ_Δ	2×10^{-6} s
Rate constant of $O_2(^1\Delta_g)$ dimolar reactions in (g)	k_Δ	3.7×10^4 m^3 kmol^{-1}s^{-1}

Two examples of calculated results for various input parameters are shown below.

Example 1

Input Data

Characteristics	**Label**	**Magnitude**
Gas entering the generator	Cl_2 + He	1 : 4
Total generator pressure	P_{tot}	40 kPa (300 torr)
Diffusion coefficient of chlorine in gas	D_{CG}	1.04×10^{-4} m^2 s^{-1}
Gas temperature	T	260 K
BHP droplet radius	a	10 μm
Initial HO_2^- concentration in BHP	c_{HL0}	3 kmol m^{-3}
Ratio of BHP/chlorine utilization	U_H/U_C	0.5

Results

Characteristics	Label	Magnitude
Volume fraction of liquid phase	λ	0.0049
Radius of gas sphere	b	59 μm
Initial flux of chlorine per unit droplet surface	j_{CsI}	1.7 mol m^{-2} s^{-1}
Initial characteristic depth of $O_2(^1\Delta_g)$ production	X_P	0.58 nm
Characteristic depth of $O_2(^1\Delta_g)$ quenching in liquid	X_{QL}	31.6 nm
Initial flux of $O_2(^1\Delta_g)$	$j_{\Delta sI}$	1.6 mol m^{-2} s^{-1}
Duration of initial (surface-limited) period	t_d	0.24 ms
Delay of the stage limited by HO_2^- diffusion	Δt	0.13 ms
Time of maximum $O_2(^1\Delta_g)$ partial pressure	t_{max}	6.2 ms
Maximum partial pressure of $O_2(^1\Delta_g)$	$p_{\Delta max}$	5.5 kPa (41 torr)
Chlorine utilization	U_C	100%
BHP utilization	U_H	50%

Fig. 4 illustrates a fast HO_2^- depletion from the BHP surface. In this period, the surface process plays a controlling role. Afterwards the overall process is controlled by HO_2^- diffusion. The end of decreasing in HO_2^- mean concentration (at t ≅ 6 ms) corresponds to exhausting time of chlorine in gas phase. In **Fig. 5**, the first part of the blue curve documents an accumulation of $O_2(^1\Delta)$ during the production period, and the declining part reflects mainly $O_2(^1\Delta)$ quenching in the gas phase. It means that singlet oxygen should exit the generator in a time of the maximum $O_2(^1\Delta)$ concentration, i.e. about 6.2 ms after droplet formation.

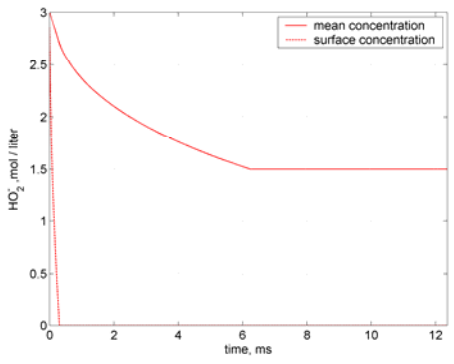

Fig. 4 Time dependence of HO_2^- depletion

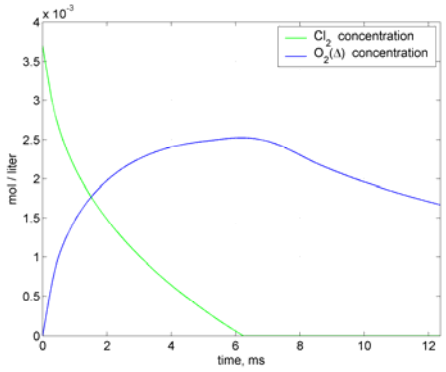

Fig. 5 Time evolution of Cl_2 and $O_2(^1\Delta)$ concentration

Example 2

This case was calculated for a higher total pressure (100 kPa (750 torr)), lower BHP concentration, and smaller droplets (d = 2a = 10 μm). The results are in **Figs. 6** and **7**.

Input data

Characteristics	**Label**	**Magnitude**
Gas entering the generator	Cl_2 + He	1 : 4
Total generator pressure	P_{tot}	100 kPa (750 torr)
Diffusion coefficient of chlorine in gas	D_{CG}	0.33×10^{-4} m^2 s^{-1}
Gas temperature	T	260 K
BHP droplet radius	a	5 μm
Initial HO_2^- concentration in BHP	c_{HL0}	2 kmol m^{-3}
Ratio of BHP/chlorine utilization	U_H/U_C	0.5

Results

Characteristics	**Label**	**Magnitude**
Volume fraction of liquid phase	λ	0.018
Radius of gas sphere	b	19 μm
Initial flux of chlorine per unit surface of droplets	j_{CsI}	4 mol m^{-2} s^{-1}
Initial characteristic depth of $O_2(^1\Delta_g)$ production	X_P	0.7 nm
Characteristic depth of $O_2(^1\Delta_g)$ quenching in liquid	X_{QL}	31.6 nm
Initial flux of $O_2(^1\Delta_g)$	$j_{\Delta sI}$	3.8 mol m^{-2} s^{-1}
Duration of initial (surface-limited) period	t_d	0.02 ms
Delay of the stage limited by HO_2^- diffusion	Δt	0.01 ms
Time of maximum $O_2(^1\Delta_g)$ partial pressure	t_{max}	1.4 ms
Oxygen pressure at this time	p_{O2}	20 kPa (150 torr)
Maximum partial pressure of $O_2(^1\Delta_g)$	$p_{\Delta max}$	15 kPa (112 torr)
Chlorine utilization	U_C	97%
BHP utilization	U_H	49%

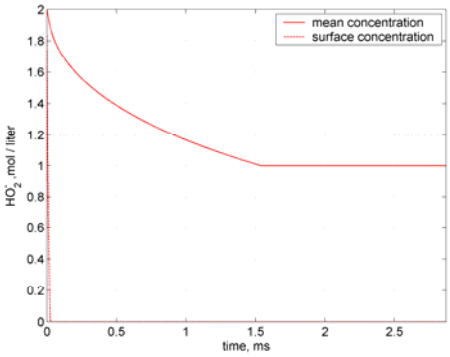

Fig. 6 Time dependence of HO_2^- depletion

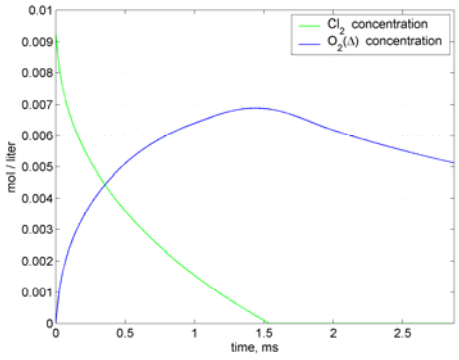

Fig. 7 Time evolution of Cl_2 and $O_2(^1\Delta)$ concentration

A comparing these results with results of the Example 1 shows that in this case, the initial flux of $O_2(^1\Delta_g)$ and its maximum partial pressure are significantly higher, and all characteristic times are substantially shorter. A maximum partial pressure of $O_2(^1\Delta_g)$ of 15 kPa (112 torr) should be achieved 1.4 ms from the beginning of chlorine contact with BHP droplets. At this time, the calculated $O_2(^1\Delta_g)$ yield is 75%.

5. Two-phase nozzles for spray formation

General considerations

The preliminary calculations showed that high partial pressures of singlet oxygen (≥ 5.5 kPa (40 Torr)) could be achieved with only very small droplets in formed BHP spray (diameter ≤ 20 μm). According to a survey of commercial nozzles available from world producers, small-droplet sprays of fairly viscous liquid (like BHP at low temperatures (10 – 50 mPas)), could be produced by nozzles atomizing liquid by pressurized gas. The air-blast atomizers have the advantage of thorough g/l mixing and production of fine sprays. In a pre-filming type nozzle, liquid is first spread out in a thin continuous sheet and then subjected to atomizing action of high-velocity gas. Two separate gas flows allow the atomizing gas to impact on both sides of the liquid sheet. The nozzle can produce either a hollow cone spray (for a shorter contact time) or a full cone spray.

The crucial factor for choosing a suitable nozzle for the proposed CentSpraySOG is the ratio of gas/liquid flow rates that ensure a time atomization. To obtain the highest Cl_2 utilization, rather low g/l ratio is needed, but to ensure a fine atomization, the gas flow rate must be as high as possible. To exclude a precipitation of the salt from BHP, which could block the nozzle orifices, the nozzles with external atomizing (mixing gas and liquid phases) are preferred. Further, a choice of the nozzle depends also on requirement for the contact time of both phases, which is determined by the

shape of the spray cone. The contact time is shorter in a hollow cone spray than in a full cone spray. The manufacturers give in their prospectus usually only data on the liquid and gas flow rate for different input pressures of liquid and gas but the data on the droplet size are given only exceptionally (and only for water and air at atmospheric pressure and for selected flow rates only).

From the performed survey of available nozzles, we consider following types of the nozzles for our planned application in the investigation of CentSpraySOG:

BETE Fog Nozzle, Inc. (50 Greenfield Street, Greenfield, MA 01301)
The SAM-type nozzles with external mixing were designed for spraying of viscous liquid yielding very fine droplets (no data on droplets diameter are given).

Tab. 4
Gas (atomizing + fan) flow rate to liquid flow rate ratio for SAM nozzles

Type	$V_{G(atom)} / v_L$,	$(v_{G(atom)} + v_{G(fan)}) / v_L$,	$(n_{G(atom)} + n_{G(fan)}) / v_L$, mmol (g)/ml (l)
SAM 05-03	0.55	0.82	13.6
SAM 06-04	0.27	0.42	6.98
SAM 07-05	0.166	0.25	4.15

Düsen-Schlick GmbH (Hutstrasse 4, 96253 Untersiemau/Coburg, Germany) Nozzles of the series 938, 848, 0/28, and 0/48 can atomize liquids to a finer degree than other two-substance nozzles; models 0/48 and 840 are designed for double air atomization.

Tab. 5
Atomizing gas flow rate to liquid flow rate for two-substance nozzles providing finest atomization

Type	v_G, Nm^3/h	v_L, l/min	n_G / v_L, mmol (g)/ml (l)
938, 0/28	11.0	0.9	9.1
938, 0/28	19.0	1.5	9.4
0/48	28	0.7	30
0/48	74	2.5	22
0/48	88	4	16

Water droplet diameter of 3.5 μm to 27 μm is given for nozzle Model 0/48 at water flow rate of 0.4 l/min, and airflow rate of 74 Nm^3/h with a spray cone angle of 120^o.

Spraying Systems CZ, s.r.o. (Kamenná 31, 639 20 Brno, Czech Rep.)

Tab. 6

Type 1/8J JAU, Internal Mix., no data on droplet size

Type	v_G, Nm^3/h	v_L, l/min	n_G/v_L, mmol (g)/ml (l)
SUJ 22DF	3.4	0.52	6.6
SUJ 22DF	6.2	1.33	3.45

For the spray SOG operation using chlorine-helium mixture in the ratio 1:4, and 2 to 8 M HO_2^- in BHP, the ratio n_G/v_L of 2.5 to 10 mmol/ml is required for attaining the BHP utilization of 0.5.

6. Model calculations for chosen nozzles

6.1. Results of parametric estimations

The model calculations for the nozzles SAM-05-03 to 07-05 with external g/l mixing and two gas inlets (for atomization gas and gas controlling the spray-cone angle) were performed. The examples below were calculated for gas and liquid flow rates that assure a fine liquid atomization. The pressure was calculated from the molar flow rate of gas and pumping speed corresponding to either the rotary pump capacity (300 m^3/h), or this capacity lowered by 2x, 3x, 4x, and 5x, respectively. For these conditions, time dependences of the surface and mean concentration of HO_2^- ions in the drop and the mean concentration of chlorine and singlet oxygen in the gas were calculated. They are shown in **Figs. 8 – 11**. The relative concentration of HO_2^- ions in Figs. 8 – 10 is related to the initial HO_2^- concentration in the bulk of BHP, the relative Cl_2 and $O_2(^1\Delta)$ concentrations in gas are related to the initial Cl_2 concentration in the gas bulk.

Figs. 8 and **9** illustrate time dependences calculated for the nozzle SAM 06-04 and for two different droplet diameters in the spray. It can be seen that HO_2^- ions on the drop surface are quickly exhausted (within 1.5 ms). The decrease in the mean HO_2^- concentration in liquid finishes after the chlorine exhausting. Neglecting the effect of limited chlorine transport rate in gas causes a sharp change in the course of Cl_2 concentration near zero. A maximum of $O_2(^1\Delta)$ concentration was achieved after 24 and 13 ms, respectively. The $O_2(^1\Delta)$ yield was still rather high at this time (Y = 0.64 or 0.7, respectively). The Cl_2 exhausting was several times faster in the finer spray (**Fig. 9**) where the specific surface area of liquid was 4times higher. The Cl_2 and BHP utilizations were also higher for the spray with smaller drops (U_C = 0.75 and U_H = 0.38).

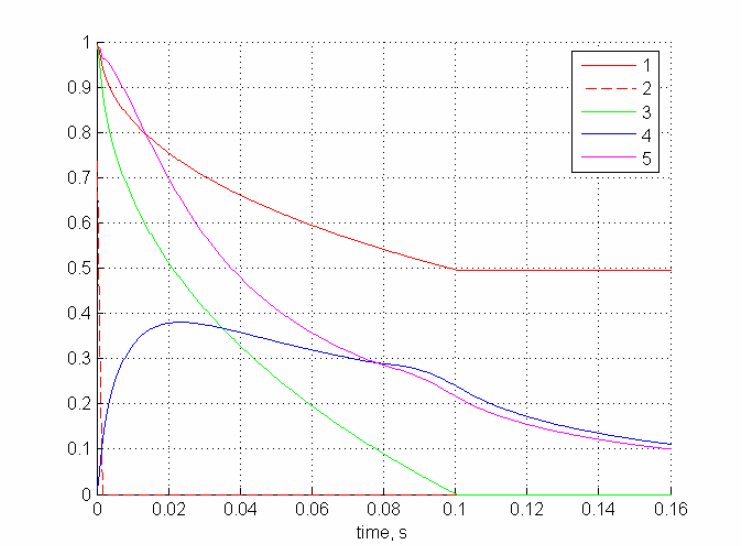

Fig. 8 Time dependence of relative mean (1) and surface (2) concentrations of HO_2^- ions for **40 μm drop**, mean concentration of Cl_2 (3) and $O_2(^1\Delta)$ (4) in gas, and $O_2(^1\Delta)$ yield (5), c_{HO2-} = 5 M, v_L = 31.7 ml/s, **n_{Cl2} = 40 mmol/s Cl_2**, Cl_2:He = 1:4, Q_{pump} = 0.016 m^3/s, P_{tot} = 32 kPa (240 torr)

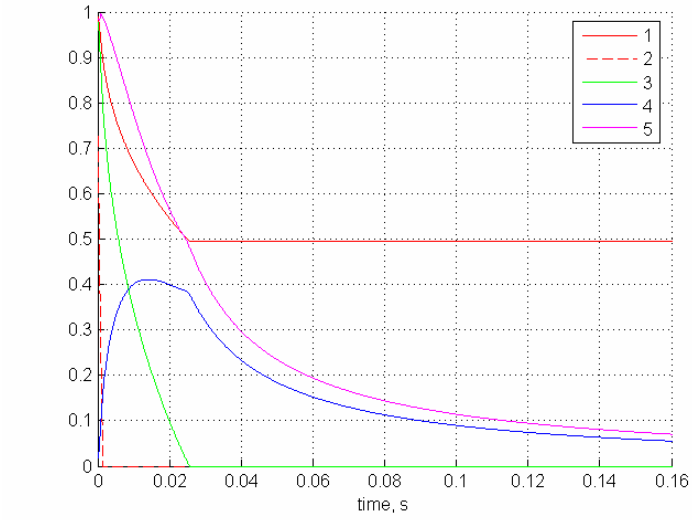

Fig. 9 Time dependence of relative mean (1) and surface (2) concentrations of HO_2^- ions for **20 μm drops**, mean concentration of Cl_2 (3) and $O_2(^1\Delta)$ (4) in gas, and $O_2(^1\Delta)$ yield (5); other conditions as in Fig. 8.

Results of calculations for a larger nozzle (SAM 07-05) and higher chlorine flow rate (and so a higher pressure), are in **Fig. 10.**

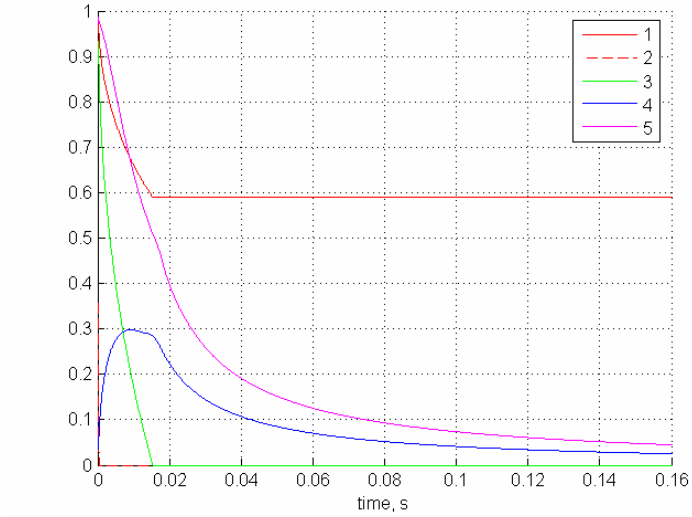

Fig. 10 Time dependence of relative mean (1) and surface (2) concentrations of HO_2^- ions for **20 μm drops**, the relative mean concentration of Cl_2 (3) and $O_2(^1\Delta)$ (4) in gas, and $O_2(^1\Delta)$ yield (5), $\mathbf{n_{Cl2} = 60\ mmol/s\ Cl_2}$, Cl_2:He = 1:4, $\mathbf{c_{HO2} = 5\ kmol/m^3}$, v_L = 58.3 ml/s, P_{tot} = 48 kPa (360 torr)

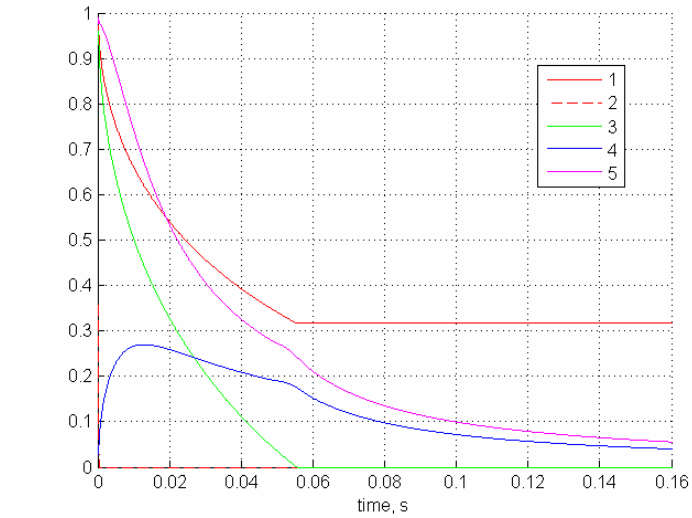

Fig. 11 Time dependence of relative mean (1) and surface (2) concentrations of HO_2^- ions for **20 μm drops**, the relative mean concentration of Cl_2 (3) and $O_2(^1\Delta)$ (4) in gas, and $O_2(^1\Delta)$ yield (5), $\mathbf{n_{Cl2} = 60\ mmol/s\ Cl_2}$, Cl_2:He = 1:4, $\mathbf{c_{HO2} = 3\ kmol/m^3}$, v_L = 58.3 ml/s, P_{tot} = 48 kPa (360 torr)

The Cl_2 utilization is higher in this case (U_C = 0.81) than in Fig. 9, which is caused mainly by a higher surface area of liquid due to the lower g/l ratio for this nozzle (see Table 4). The BHP utilization is slightly lower (U_H = 0.34) than in Fig. 9, but it could be higher for less concentrated BHP (3 M HO_2^-) (**Fig. 11).** The chlorine utilization is then however lower.

It should be mentioned that the results of calculations above are rather tentative because of the real drop size of the BHP produced by these nozzles is approximate only, and more reliable information about this parameter must be obtained experimentally. Planned measurements on the drop size will be performed first with a model solution of the same viscosity like BHP (NaOH or glycerin), and then with BHP at the temperature used for the COIL operation.

Pressure dependence of the spray SOG parameters

Example 1

This calculation was performed for different Cl_2 flow rates and one BHP flow rate using the nozzle SAM 06-04. The results correspond to the time of maximum $O_2(^1\Delta)$ partial pressure and are shown in **Figs. 12 a, b, c**.

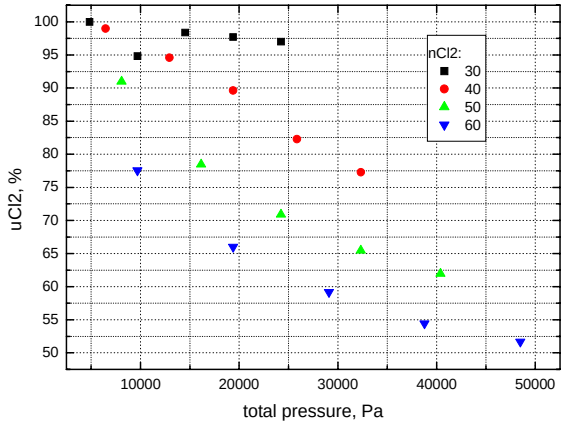

Fig. 12 a

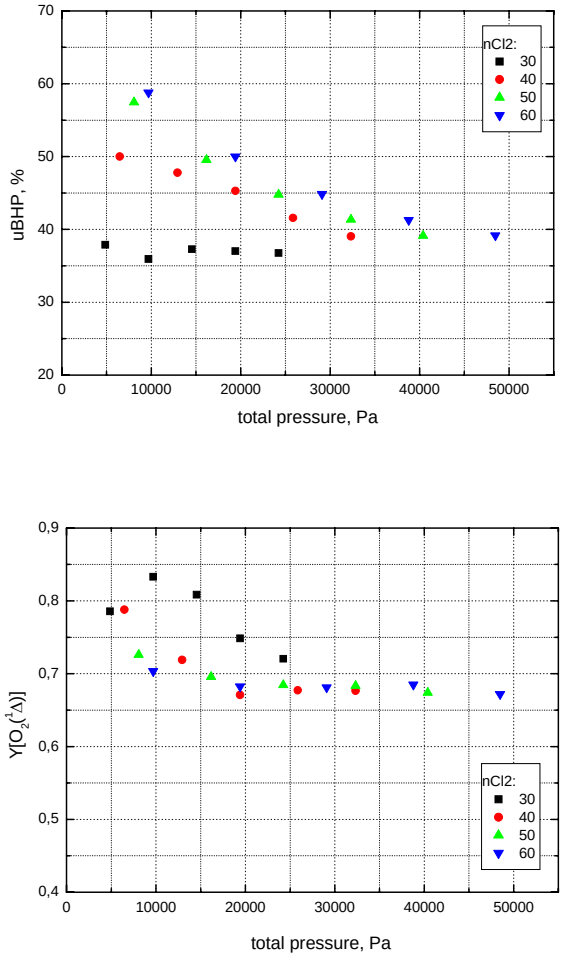

Figs. 12 a, b, c Dependence of chlorine, BHP utilization, and $O_2(^1\Delta)$ yield on total pressure; nozzle SAM 06-04, d = 40 μm, v_L = 31.7 ml/s, n_{Cl2} = 30 – 60 mmol/s Cl_2, x_{Cl2} = 0.2 (Cl_2:He = 1:4), c_{HO2-}= 5 kmol/m^3

A decrease in U_{Cl2} with increasing pressure can be explained by a higher $O_2(^1\Delta)$ loss in gas at higher pressure. At higher pressure, the maximum concentration of $O_2(^1\Delta)$ is achieved at lower degree of Cl_2 conversion to $O_2(^1\Delta)$. Chlorine utilization U_C declines markedly with increasing n_{Cl2} at constant pumping velocity. This decrease is much stronger than it would be correspond to the pressure effect. The BHP utilization (U_H) weakly increases with increasing Cl_2 flow rate. The $O_2(^1\Delta)$ yield decreases with pressure at p<25 kPa (~200 Torr). A negligible effect of pressure on the $O_2(^1\Delta)$ yield observed at pressures above 25 kPa (**Fig. 12c)** is difficult to explain because every point relates to a maximum

$O_2(^1\Delta)$ concentration, not to either constant reaction time or reactor volume. In this example, the highest partial pressure of oxygen was 4 – 5 kPa (30 – 37 Torr) at medium $O_2(^1\Delta)$ yield of 0.68.

Example 2

This calculation was performed for various dilutions of chlorine with helium with constant chlorine flow rate in the nozzle SAM 06-04. At a lower molar fraction of chlorine, the He flow rate was higher resulting in a higher total pressure, while U_C remained constant. This is due to neglecting mass-transfer constrains in the gas phase applied in this model. The results are presented in **Figs. 13 a, b**.

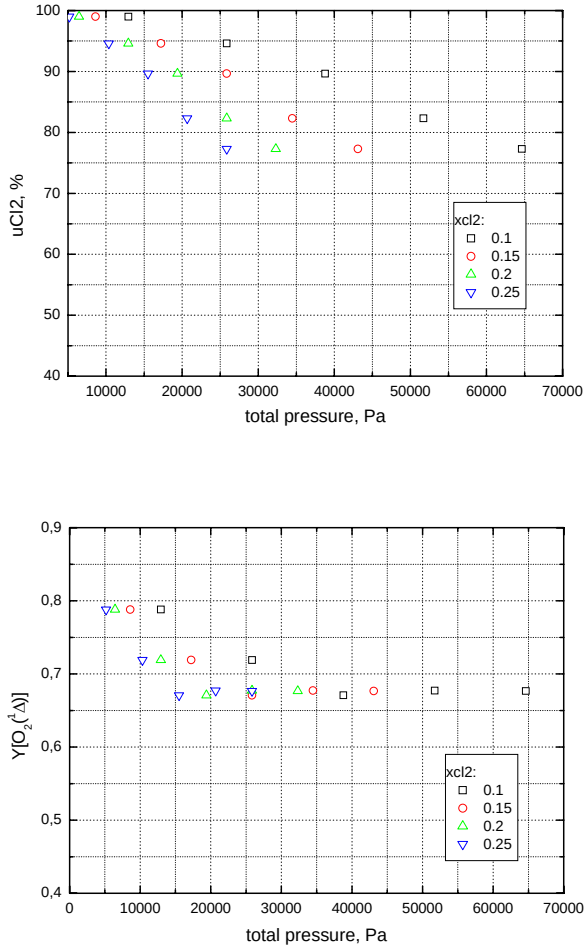

Fig. 13 a, b Dependence of chlorine utilization, and $O_2(^1\Delta)$ yield on total pressure; nozzle SAM 06-04, d = 40 μm, v_L = 31.7 ml/s, n_{Cl2} = 40 mmol/s Cl_2, x_{Cl2} = 0.1 – 0.25, i.e., n_{He} = 120 – 360 mmol/s, c_{HO2-}= 5 kmol/m^3

Example 3

In this calculation, the effect of BHP concentration was examined. The results are shown in **Figs. 14 a, b**.

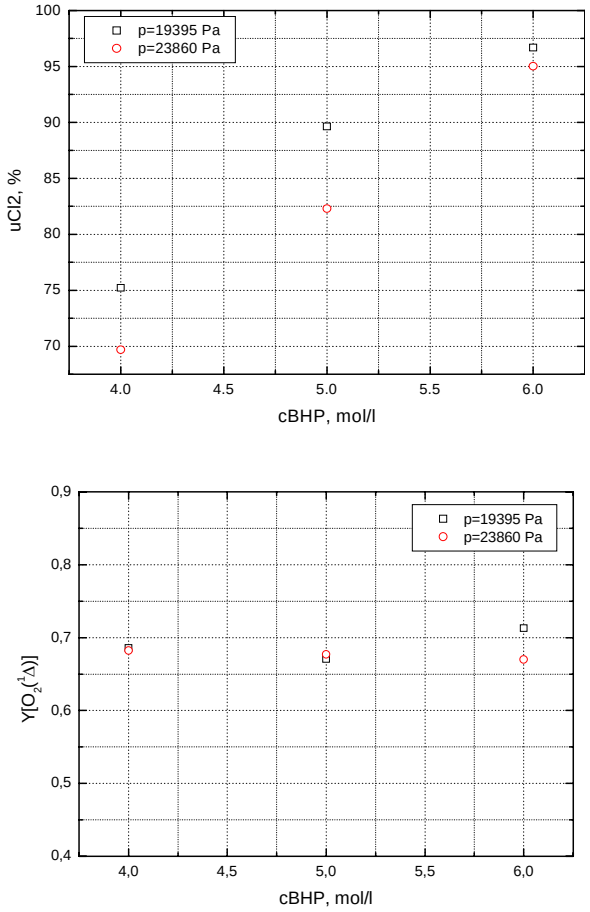

Fig. 14 a, b. Dependence of chlorine utilization, and $O_2(^1\Delta)$ yield on BHP concentration at two different pressures ; nozzle SAM 06-04, d = 40 μm, v_L = 31.7 ml/s, n_{Cl2} = 40 mmol/s Cl_2,

The increasing U_C with increasing HO_2^- concentration is caused by the effect of HO_2^- mass transfer rate controlling the rate of $O_2(^1\Delta)$ formation in the final stage (see the chap. 3). The $O_2(^1\Delta)$ yield is nearly independent of the HO_2^- concentration.

Example 4

This example is calculated for a larger nozzle (SAM 07-05) making possible higher flow rates of BHP at the same gas glow rate, and so a higher ratio of liquid/gas volume. The results are in **Figs. 15 a, b**.

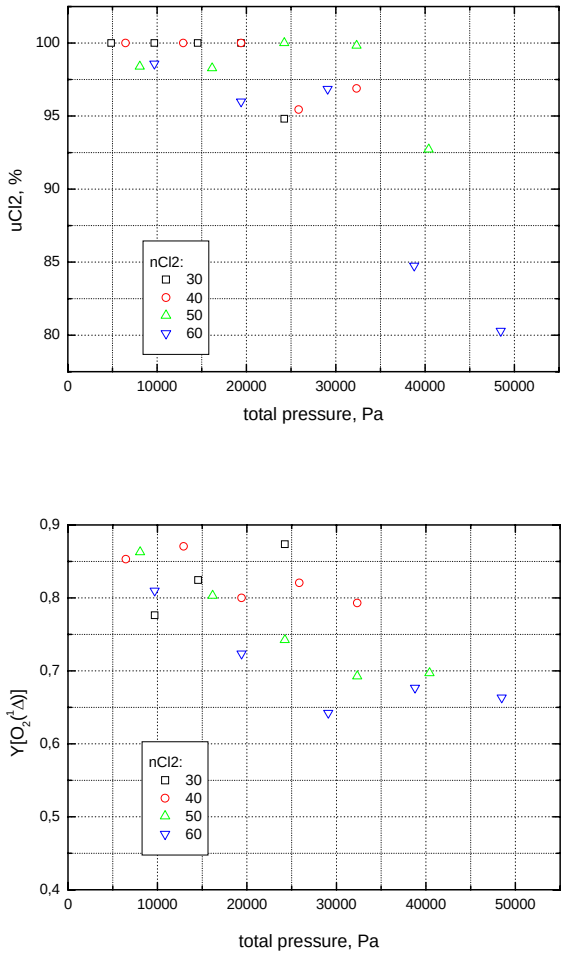

Fig. 15 a, b Dependence of chlorine utilization, and $O_2(^1\Delta)$ yield on total pressure; nozzle SAM 07-05, d = 40 μm, v_L = 58.3 ml/s, n_{Cl2} = 30 - 60 mmol/s Cl_2, x_{Cl2} = 0.2, c_{HO2-}= 5 kmol/m^3

In comparison with Example 1, a higher U_C can be achieved for the same gas flow rate and pressure. This can be explained by a higher number of droplets and their larger specific surface. The O_2 partial pressure of 5 – 7.7 kPa (38 – 58 Torr) with $O_2(^1\Delta)$ yield of 0.65 – 0.8 was calculated.

Example 5

This calculation shows the effect of droplet size in the spray on the Cl_2 utilization and $O_2(^1\Delta)$ yield (4times higher specific surface area of liquid vs. Example 1). The results are in **Figs. 16 a, b, c**.

Fig. 16c illustrates the dependence of effective reactor volume on the pressure at Cl_2 molar flow rates that could be sufficient for 1 kW-class COIL. It can be seen that the reactor volume is relatively small (up to 100 cm^3) at pressures of 24 – 48 kPa (180 – 360 Torr). The cylindrical reactor of 5 cm in diameter could be then only 5 cm long. The calculated O_2 partial pressure would be 4.8– 9 kPa (36 – 67 Torr) at the $O_2(^1\Delta)$ yield exceeding 0.8.

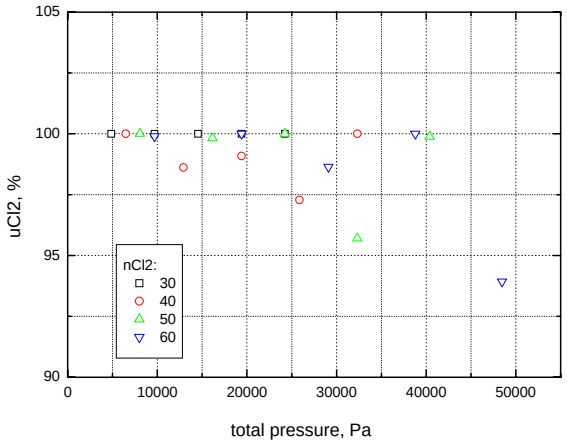

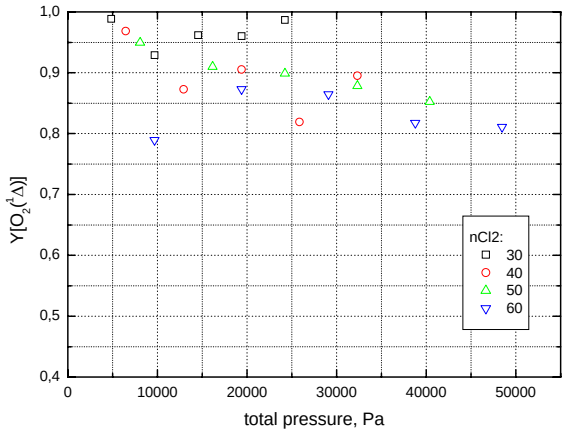

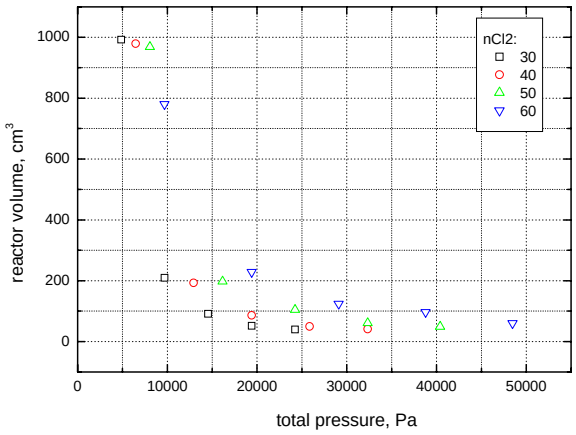

Fig. 16 a, b, c Dependence of chlorine utilization, $O_2(^1\Delta)$ yield, and reactor volume on total pressure; nozzle SAM 07-05, d = 20 μm, v_L = 58.3 ml/s, n_{Cl2} = 30 - 60 mmol/s Cl_2, x_{Cl2} = 0.2, c_{HO2^-}= 5 kmol/m^3

Limitation of the present model

The model used for the above calculations was based on several assumptions, which may result in differences between its prediction and experiment. They are:

1/ Infinite mass transport rate in the gas phase:

This assumption becomes incorrect when the chlorine utilization reaches 100%. At that time, the transport limitation in gas arises and the real utilization would be slightly lower then predicted.

2/ Perfect "co-flow" of gas and liquid phases

In the real situation, the velocity of gas and liquid droplets can be different, especially during the initial stage. Droplets could also coagulate to some extent. Both these effects can result in a surface renewal and so enhancement of the mass transfer towards and backwards the droplet. This effect causes a faster Cl_2 utilization and can thus extend a time for singlet oxygen quenching. Quantitative evaluation of the impact of surface renewal on the generator performance can be estimated only experimentally.

3/ The rate of $O_2(^1\Delta)$ quenching in the liquid phase

The above calculations included the value of $O_2(^1\Delta)$ lifetime in BHP of 2 x 10^{-6} s given in the literature. Blauer at al. [1] found by comparison between their model and experiments that the liquid phase quenching could be higher by two orders of magnitude than corresponds to the literature value. Based on this estimation, the $O_2(^1\Delta)$ yields evaluated from our modeling can be treated as the upper limit values.

4/ Uniform droplet size

The real spray will have a certain distribution in the droplet size. The results on Cl_2 utilization and yield are "correct" for the mean droplet radius included in the model calculations, but the droplet size distribution must be taken into account when the model counts also with the enthalpy balance. The present model does not predict yet the heat release and convection, and consequently the amount of water vapor content in the gas. It is obvious that smaller droplets will evaporate faster and so produce more water vapor.

6.2. Conclusions from the modeling

- The calculations performed for chosen nozzles producing the BHP spray with 40-μm or 20-μm droplets show that $O_2(^1\Delta)$ can be generated by the CentSpraySOG of a small inner volume 100 cm^3, at the oxygen pressure of 4.8– 9 kPa (36 – 67 Torr), and with the $O_2(^1\Delta)$ yield exceeding 0.8. The SOG with these parameters would be satisfactory for driving a 1 kW-class COIL. The above calculations were performed for rather concentrated BHP solutions (with 3–7 M HO_2^-) because the chosen small two-phase nozzles need a relatively high g/l ratio.
- Even higher $O_2(^1\Delta)$ partial pressure (20 kPa (150 torr)) could be achieved employing a spray with smaller droplets, but production of such sprays could be difficult due to the high BHP viscosity at low temperature. This problem could be solved by using higher flow rates of more diluted BHP, which would be advantageous also for the lower temperature increase during the reaction with chlorine. A needed lowering the gas/liquid ratio can be obtained easier by using larger nozzles. Temperature of the two-phase mixture could be lowered also by some cooled liquid (e.g., a cooled diluted H_2O_2 or some non-freezing and non-reactive solution), which would be sprayed from another nozzle downstream of the reaction region. After this cooling, the two-phase mixture would enter the centrifugal separator.

7. Experimental set-up for measuring a drop size and drop velocity

7.1. Methods available for these measurements

Methods employed in a drop size measurement may be grouped into three categories: mechanical, electrical and optical. The optical methods are either droplet imaging (photography, holography) or droplet non-imaging (e.g. Phase Doppler Anemometry). Some of them are briefly described below.

High-speed photography

This technique is rather simple utilizing a flashlight or laser pulse to create a high intensity and short-time light source. Duration of the flashlight should be of the order of 1 μs, and the laser pulse of the order of nanoseconds. It can be used also for getting the information about drop velocities. This technique is not very convenient because of time-consuming.

Light-scattering interferometry

Drop size and velocity measurement is based on the observation of light scattered by drops flying through the crossover region of two intersecting laser beams. The drop velocity is calculated as

$$U = \lambda f_D/(2 \sin(\theta/2))$$

where λ is the wavelength of laser light, f_D the Doppler frequency, and $\theta/2$ laser beam intersection half-angle. A size information is contained in the relative modulation (visibility) of the scattered signal. Based on the scalar diffraction theory, the relationship between drop size and visibility can be expressed as

$$\text{Visibility} = 2 J_1(\pi D/\delta)/\pi D/\delta$$

where D is drop diameter, J_1 the first-order Bessel function, and δ the interference fringe spacing.

Phase Doppler Particle Analysis

Theoretical description of the dual-beam light scattering showed that the spatial frequency of the scattered interference fringe pattern at off-axis angle is inversely related to a drop diameter. The method uses pairs of detectors at fixed spacing in the image of interference or fringe pattern. The overall measurement size range is from 1 μm to several thousands μm, and can be used also for dense sprays.

Malvern Particle Sizer

The device uses a method based on the Freuenhofer diffraction of parallel beam of the monochromatic light by a moving drop. A diffraction pattern is formed, in which part of the light is diffracted depending on the drop size. This commercial technique is very effective, relatively simple and reliable.

The instrumentation of the optical methods is rather expensive and their use needs some experience. It requires calibration with highly mono-dispersed droplets that are either sprayed from a dilute liquid suspension and subsequently dried or present in liquid suspensions.

We plan to employ initially the high-speed photography for exploration of the spray produced by different nozzles. In the next investigation, some non-imagine optical method would be probably necessary.

7.2. Scheme of device for spray parametric study

The device consists of a cooled liquid reservoir connected by a valve with the spray-nozzle. The liquid will be compressed by nitrogen delivered through tube in the upper part. The nozzle is fed by atomizing gas (N_2 or He) producing a spray in the low-pressure chamber evacuated by rotary pump (300 m^3/h). Side mirrors of the chamber for the droplet size investigation by the diagnostic beam are purged by means of nitrogen (or He).

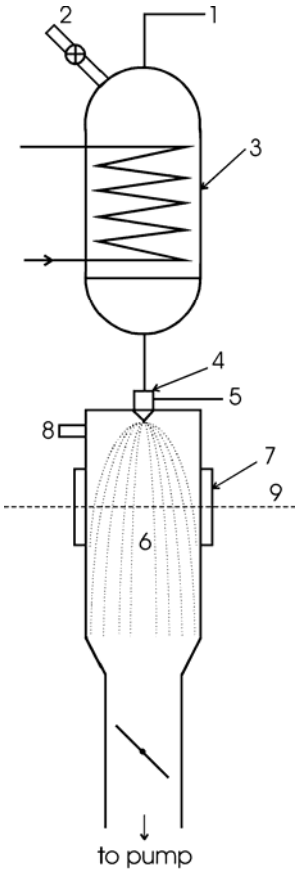

Fig. 20. Scheme of device for spray studies
1 - pressurized N_2 (He)
2 – inlet of tested liquid
3 – tank for tested liquid
4 – nozzle
5 – atomizing N_2
6 – diagnostic chamber
7 – diagnostic window
8 – inlet of purging N_2
9 – diagnostic beam

8. Design of gas/liquid blade separator for CentSpraySOG

8.1. Geometry of channels between next blades in separator

The separator is formed by rotor with radial spiral blades. The centrifugal acceleration of the blades is

$$a = \omega^2 r \qquad (53)$$

where ω is angular velocity (rad/s) and r is radius. The angular velocity is related to a number of revolutions per minute (r.p.m.) as

$$\omega = 2\pi \text{ r.p.m.} / 60 . \quad (54)$$

The centrifugal acceleration can be decomposed into a component tangential to the blade

$$a_t = a \cos \alpha , \quad (55)$$

and a component normal to the blade

$$a_n = a \sin \alpha . \quad (56)$$

Here α is angle between the tangent of the blade and the radial coordinate.

It is proposed that the blade shape is spiral with polar angle θ, being a function of the radial coordinate r

$$\theta = \theta_{in} - \tan \alpha_{in} - \arctan (1/\tan \alpha_{in}) + (\rho^2 - 1)^{1/2} + \arctan (1/(\rho^2 - 1)^{1/2}) \quad (57)$$

Symbols θ_{in}, α_{in}, and r_{in} relate to respective parameters at the inner radius of the blade.

Here ρ is a dimensionless radial coordinate

$$\rho = r/q , \quad (58)$$

where

$$q = r_{in} / (1 + \tan^2 \alpha_{in})^{1/2} \quad (59)$$

The angle between the blade tangent and radial coordinate is

$$\alpha = \arctan (\rho^2 - 1)^{1/2} . \quad (60)$$

The length of the blade contour between radii r_{in} and r is

$$L(r) = (r^2 - r_{in}^2) / 2q . \quad (61)$$

This spiral blade has two remarkable properties:

i) The tangential acceleration is constant along the blade surface

$$a_t = \omega^2 q , \quad (62)$$

which ensures a driving of the BHP film with constant force.

ii) The height h of the channel formed by adjacent blades is constant

$$h = \Delta\theta r \cos \alpha = \Delta\theta q \quad (63)$$

where $\Delta\theta$ is a difference of polar angles of adjacent blades of the same radius.

8.2. Hydrodynamics of flowing film along blades

The initial approximation for the flow of liquid along the blade is made for the assumption that most liquid is separated from the g/l mixture at the entrance into the blade space. The relation for the tangential velocity, v(x) was taken from [3] by replacing the gravitational acceleration g with the centrifugal acceleration a

$$v(x) = [(\rho a\delta^2 \cos \alpha)/2\mu] [1 - (x/\delta)^2] = [(\rho \omega^2 q\delta^2)/2\mu] [1 - (x/\delta)^2] , \quad (64)$$

where x is the coordinate normal to the blade (ranging from 0 at the liquid/gas interface to δ at the liquid/blade interface), μ is dynamic viscosity of the liquid.

Maximum velocity at x = 0 is

$$v_{max} = (\rho\, \omega^2\, q\delta^2) / 2\mu \ . \quad (65)$$

Average velocity is $$v_{av} = 2/3\ v_{max} = (\rho\, \omega^2\, q\delta^2) / 3\mu \ . \quad (66)$$

Volumetric flow rate per one blade of width *w* is

$$V_l = w\, \delta\, v_{av} = (w\rho\, \omega^2\, q\delta^3) / 3\mu \ . \quad (67)$$

Average retention time τ_{av} is

$$\tau_{av} = L(r) / v_{av} \ . \quad (68)$$

Depending on the Reynolds number

$$\mathrm{Re} = 4\delta\, v_{av}\, \rho / \mu \quad (69)$$

three regimes of the flow can be recognized:

- Re < 20: laminar flow with negligible ripping. Here the analysis is fully valid.
- 20 < Re < 1500: laminar flow with pronounced rippling. Here the analysis can be good for approximation.
- Re > 1500: turbulent flow. The analysis is not valid.

8.3. Settling (disengagement) of droplets

Mean displacement due to the Brownian motion is

$$x_{rms} = (2\, D_p\, t)^{1/2} \quad (70)$$

where the diffusion coefficient of the particle (drop) is given as

$$D_p = kTC_c / 3\pi\eta d_p \ . \quad (71)$$

C_c is the Cunningham correction factor, expressing the velocity slip between the particle and gas. The terminal settling velocity of a particle is

$$v_{TS} = \rho_p d_p^2 a_n\, C_c / 18\eta \ . \quad (72)$$

Average distance travelled due to a settling is

$$x_S = v_{TS}\, t = \rho_p d_p^2 a_n C_c t / 18\eta \ . \quad (73)$$

Efficiently removed are particles for which

$$x_S > x_{rms}\ , \quad (74)$$

having a diameter $$d_p > [(kT\eta)/(\rho_p a_n C_c t)]^{1/5} \quad (75)$$

8.4. Geometry of liquid separator and parameters of liquid film

Dimensions of the rotor of the centrifugal blade separator are given in **Table 7**

Tab. 7

Rotor inner diameter,	d_{in} = 50 mm
Channels number	n = 6
Channel width	w = 50 mm
Channel length	l = 100 mm
Blade revolutions per minute	n = 1000 – 16000 r.p.m.

Parameters of liquid film

Some examples of the calculated effect of BHP flow rate on the film thickness, the mean velocity of liquid, and the BHP retention time were presented in Figs. 5 – 7 of the interim Report 001. **Table 8** gives the film thickness calculated for rotor parameters from the Table 7, the total BHP flow rate of 58.3 ml/s (assumed for the nozzle SAM 07-05 in the Examples 4,5 in chap. 6.1.), and BHP viscosity of 20 mPas.

Tab. 8
Thickness of BHP film on the separator blades

rpm, min^{-1}	1000	2000	4000	8 000	16 000
δ, mm	0.4	0.2	0.12	0.09	0.06

The calculated BHP layer in Table 8 is rather thin obviously due to its high tangential acceleration.

Separation of droplets from the spray

Table 9 gives the calculated minimum diameter of droplets that should be separated in the designed separator in dependence on rotation speed. A height of the free space in the channel for the gas flow is 1 mm obtained by subtracting the film thickness from the total channel height. The calculation was performed for the total gas pressure of 50 kPa (375 Torr).

Tab. 9
Minimum diameter of droplets ($d_{p,min}$, μm) separated by CentSpraySOG

rpm, min^{-1}	1000	2000	4000	8 000	16 000
$d_{p,min}$, μm	2.8	1.8	1.1	0.67	0.33

It is obvious that even small droplets could be separated very efficiently in the proposed centrifugal separator at revolutions above 4000 r.p.m.

8.5. Calculation of gas pressure loss in the channel

- The mean height of the free space in the channel for gas flow, h_G = 0.8 mm
- Total volumetric gas flow rate (60 mmol Cl_2 (O_2)/s and 240 mmol He_{prim}/s) at temperature 260 K, and total pressure 50 kPa (375 torr):

$$V_{G,tot} = nRT/P = 0.3\ R\ 260/50000 = 1.3 \times 10^{-2}\ m^3/h$$

- Total free cross-section for gas flow in 6 channels (w = 50 mm, h_G = 0.8 mm):

$$A_{G,tot} = 6 \times 0.05 \times 8x10^{-4}\ m^2 = 2.4 \times 10^{-4}\ m^2$$

- Gas velocity in the channel

$$v_{G,1} = V_{G,tot} / A_{G,tot} = 54.2\ m/s$$

- Reynolds number $Re_{G,1} = v\ d\ \rho_G / \mu_G$,

where gas density $\rho_G = P\ M_{av} /(RT) = 50000 \times 0.0096/(8.314 \times 260) = 0.222\ kg/m^3$

molecular weight $M_{av} = (60 \times 0.032 + 240 \times 4x10^{-3})/200 = 9.6 \times 10^{-3}\ kg/mol$

gas (O_2+ 4He) viscosity $\mu_G = 1.87x10^{-5}\ Pa\ s$

$$Re_{G,1} = vd\rho_G/\mu_G = 54.2 \times 08x10^{-3} \times 0.222 / 1.87x10^{-5} = 515$$

$$\Rightarrow \textbf{ laminar flow}$$

- **Pressure loss in a channel between blades** (laminar flow in a rectangular channel):

$$\Delta P_{G,1} = 4\ v\ l\ \mu/(w\ h_G\ k)$$

$k = 0.3\ h_G/w = 6 \times 10^{-3}$ (tabled value of the coefficient 0.3 is valid for $h_G/w = 0.02$)

The estimated pressure loss $\Delta P_{G,1}$ = $4 \times 54.2 \times 0.1 \times 1.87x10^{-5} / (0.05 \times 0.8x10^{-3} \times 6x10^{-3})$

= 1688 Pa ≅ **1.7 kPa**

is acceptable, being about 3% of the total pressure in the generator.

Calculation of $O_2(^1\Delta)$ loss in the separator

The deactivation of $O_2(^1\Delta)$ in the gas phase goes through energy pooling

$$O_2(^1\Delta) + O_2(^1\Delta) \rightarrow O_2(^1\Delta) + O_2(^3\Sigma) \qquad k_x = 2.7x10^{-17}\ cm^3/s \qquad (76)$$

and self quenching

$$O_2(^1\Delta) + O_2(^1\Delta) \rightarrow O_2(^3\Sigma) + O_2(^3\Sigma) \qquad k_y = 1.7x10^{-17}\ cm^3/s \qquad (77)$$

The effect of $O_2(^1\Delta)$ quenching can be expressed as

$$Y^{-1} = (Y_o)^{-1} + k_{tot}\ \chi \qquad (78)$$

where Y is the $O_2(^1\Delta)$ yield at the beginning and Y_o the yield at the exit,

$$k_{tot} = k_x = 2\ k_y \ , \qquad (79)$$

and

$$\chi = (P_{tot})^2\ n_{O2}\ V/(n_{tot}\ R\ T)^2 \qquad (80)$$

Data for the separator with 6 gas channels: P_{tot}=50 kPa, n_{O2}=0.060 mol/s, n_{tot}=0.3 mol/s

$V=6 \times 0.1 \times 0.05 \times 8\times10^{-4} = 2.4 \times 10^{-5}$ m^3 (volume),

$V_{G,tot}=1.3\times10^{-2}$ m^3/h (volumetric flow rate), and T=260 K

Gas retention time in a channel of the length l=0.1 m

$$\tau_{G,l} = l/v_{G,l} = 0.1 / 54.2 \cong 1.84 \text{ ms}$$

The factor χ calculated from (80) equals to

$$\chi = 8.56 \times 10^{-3} \text{ mol s/m}^3 = 5.15 \times 10^{15} \text{ molec s/cm}^3,$$

the product $k_{tot}\,\chi$ is then

$$k_{tot}\,\chi = 0.314$$

and the $O_2(^1\Delta)$ yield at the separator exit is

$$Y = 0.64.$$

This yield value is acceptable, although the $O_2(^1\Delta)$ loss should be still reduced (the product $P\tau$ is 0.138 torr s). Either smaller height of the gas channel or a shorter channel length could reduce the $O_2(^1\Delta)$ loss.

9. Design concept of CentSpraySOG device

A cross-section of the rotor of separator was schematically shown in Fig. 3. The perpendicular cross-section of this separator is given on **Fig. 21**. The rotor consists of two profiled wheels connected (by welding) by six blades. Channels for gas and BHP flow are formed between these blades of the curved shape, see calculations in chap. 8.2.). The reactor inner space is separated from the outer atmosphere by aerodynamic seals formed by a narrow labyrinth gap between rotor and stator. The rotor is connected with the electromotor by a shaft. This motor on one side and a bearing on the other side are protected by purging with nitrogen or helium. The purging gas, which flow rate is much smaller than a gas flow through the nozzle, streams through the labyrinth seal and exits into the reaction space. The shape of trajectory of droplets is affected by the pressure loss in the channels between rotor blades. The higher is this loss, the more uniform is the g/l flow along the blade width.

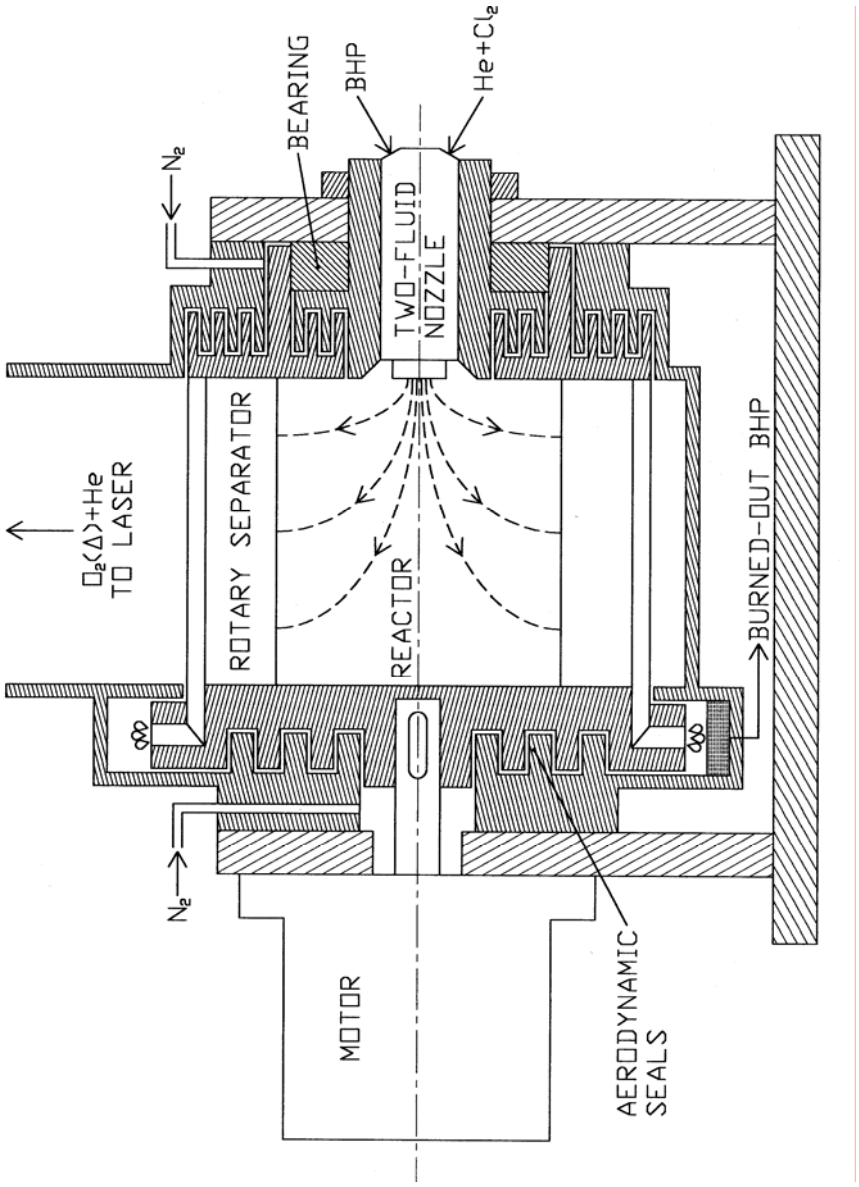

Fig. 21 Scheme of CentSpraySOG

Dimensions of the CentSpraySOG for about 1 kW COIL are given in the Table 7. The inner diameter and length of the reactor rotor can be significantly increased for attaining higher flow rates of singlet oxygen. The increase in the rotor length is limited by a need of the comparable droplet delay in the inner space for various trajectories.

Fig. 22 shows schematically a possible arrangement of several modules of CentSpraySOG with the outlet into one supersonic laser COIL nozzle.

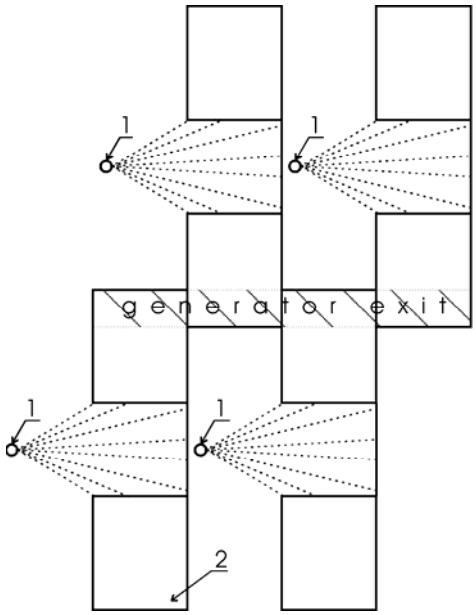

Fig. 22 Multi-module CentSpraySOG; 1- spray nozzle, 2- separator body

10. Conclusions of present study on SprayCentSOG

A summary of the results follows the requirements on the advanced SOG characteristics (Objects and goals, p. 4).

1. "*A high pressure operation with ~ 100 torr O_2 partial pressure*": By our calculations, this parameter could be fulfilled in the proposed CentSpraySOG operating with a droplet spray containing drops less than 20 μm. The calculated chlorine utilization should be above 0.95 and $O_2(^1\Delta)$ yield above 0.75 (see Example 2 in chap. 4, Example 5 in chap. 6.1).
2. "*A single BHP pass burn down*": The BHP utilization of 0.34 – 0.38 can be attained for the 5 M solution of HO_2^- ions, which is one order of magnitude higher utilization than for the jet SOG. Even higher utilization could be attained using more diluted solutions, which needs however to employ nozzles for higher flow rate of liquid (i.e., a lower ratio of gas/liquid flow rate).

3. "*A close coupling of the generator to the nozzle plenum to minimize $O_2(^1\Delta)$ losses*":
   The CentSpraySOG is designed for a direct coupling to the laser nozzle. Our calculations were focused also on estimation of the optimal reactor and separator volume. Fig. 16c illustrates that these requirements are very restrictive. In the reactor volume of ~100 cm^3, the $O_2(^1\Delta)$ yield exceeding 80% could be achieved at chlorine flow rate of 50 – 60 mmol/s and oxygen pressure of 36 – 67 Torr. The calculated overall $O_2(^1\Delta)$ yield at the exit from the separator including the reactor (100 cm^3) and separator (45 cm^3) was 64%.
4. "*An efficient disengagement of gas/liquid mixture*": By our calculations, this process could be efficiently attained by a centrifugal blade separator designed for the CentSpraySOG. At revolutions over 4000 r.p.m., droplets less than ~1 μm should be removed from the gas stream.
5. "*A scalability to be suitable for the airborne and mobile application*": One module of the CentSpraySOG can be scaled-up to increase production rate of $O_2(^1\Delta)$ by simultaneous increase in the gas and liquid flow rate, the reactor volume and the rate of generation exhausting. A choice of suitable spray nozzles is very broad, and larger two-phase nozzles can even deliver a higher liquid/gas volume ratio. For the need of airborne application, more modules of the CentSpraySOG could be coupled to one laser nozzle (see Fig. 22).

References

[1] J.A. Blauer, S.A. Munjee, K.A. Truesdell, E.C. Curtis, J.F. Sullivan, *J. Appl. Phys.* **62**, 2508 (1987)

[2] H.S. Carlslaw, J. C. Jaeger, *Conduction of heat on solids*, Oxford University Press, NY, 1959

[3] R. Byron Bird, Warren E. Stewart, and Edwin N. Lightfoot: *Transport Phenomena*, pp. 42-47, John Wiley, NY, second edition, 2002

Deleted: 9

Acknowledgement

The investigators are very grateful to the USAF EOARD for the financial support of this work, and thank Dr. Donald Smith, Program Manager, and Mrs. Beth Wann at the EAORD for their assistance and help with the grant arrangements.

We thank Dr. Gordon D. Hager, the grant supervisor, at the US AFRL/DE at the Kirtland AFB, NM, for his encouragement in our work, and beneficial discussions on the grant tasks.